POLITECNICO MILANO 1863 | DIPARTIMENTO DI ELETTRONICA INFORMAZIONE E BIOINGEGNERIA

ELLIIT 15 years

Radio Imaging and Multi-band Sensing as Enablers of 6G and Beyond

Dario Tagliaferri

21.04.2026

Outline

1. **Radio imaging in ISAC systems**
   - Brief recall of fundamentals
   - Methods (linear and non-linear)
   - Coherent multistatic imaging and integration into ISAC

2. **Multi-band sensing at FR3**
   - Motivation, potential and challenges
   - Frequency anisotropy characterization
   - Multi-band ranging

Outline

1. **Radio imaging in ISAC systems**
   - ➢ Brief recall of fundamentals

Motivation for Imaging

Localization: state estimation of targets

Estimation theory

MSE, Cramér-Rao bound (CRB), ZZB, …

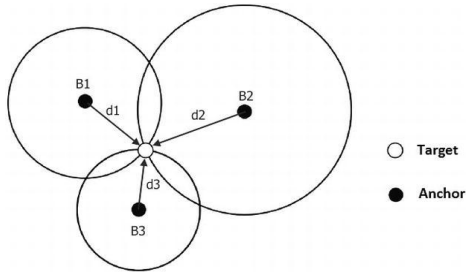

We look for **accuracy**

- ✓ Position
- ✓ Velocity
- ✓ Orientation
- ❑ Shape

Imaging: (complex) mapping of the environment

Physics

Scattering Theory

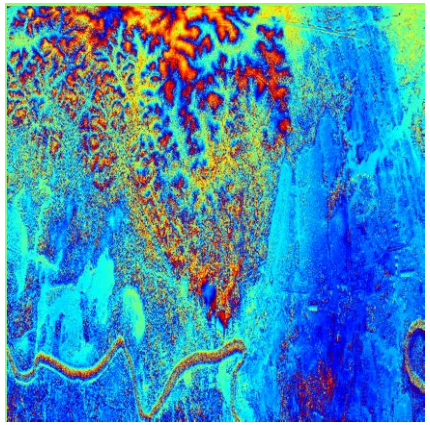

We look for **resolution**

- ✓ Position
- ✓ Velocity
- ✓ Orientation
- ✓ Shape

- N. Gonzalez-Prelcic, D. Tagliaferri, M. F. Keskin, H. Wymeersch, and L. Song, "**Six integration avenues for ISAC in 6g and beyond**," IEEE Vehicular Technology Magazine, vol. 20, no. 1, pp. 18–39, 2025
- M. Manzoni, D. Tagliaferri, S. Tebaldini, M. Mizmizi, A. V. Monti-Guarnieri, C. M. Prati, and U. Spagnolini, "**Wavefield networked sensing: Principles, algorithms, and applications**," IEEE Open Journal of the Communications Society, vol. 6, pp. 181–197, 2025.
- K. Zhi, T. Yang, S. Li, Y. Song, A. Rezaei, and G. Caire, "**Near-field integrated imaging and communication in distributed MIMO networks**," 2025. [Online]. Available: https://arxiv.org/abs/2508.17526

Motivation for Imaging

The fundamental KPI for radio imaging is RESOLUTION

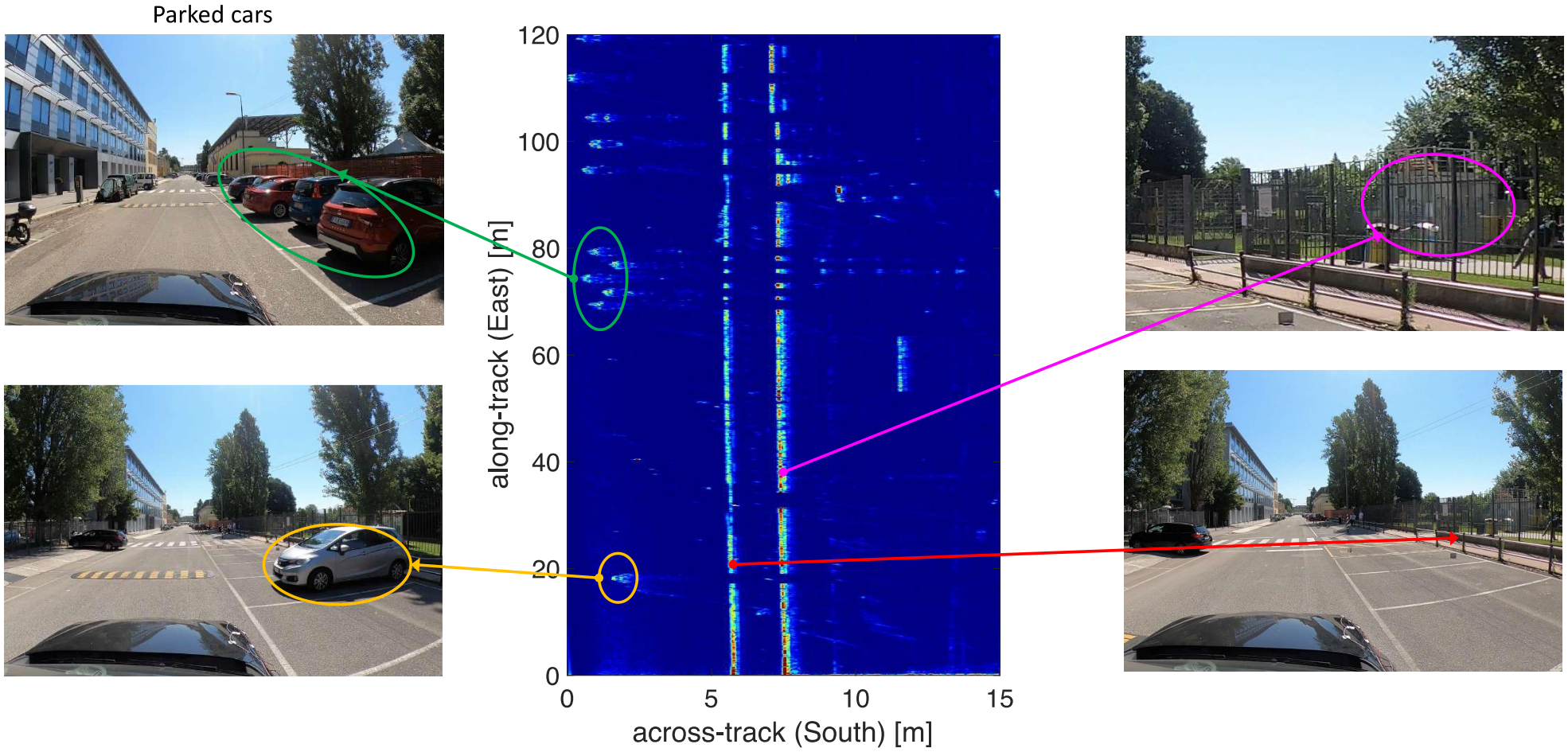

D. Tagliaferri *et al.*, "**Navigation-Aided Automotive SAR for High-Resolution Imaging of Driving Environments**," in *IEEE Access*, vol. 9, pp. 35599-35615, 2021, doi: 10.1109/ACCESS.2021.3062084

Imaging: inverse scattering reconstruction

Let us get back to scattering physics

Imaging: reconstruct the object from the scattered wave

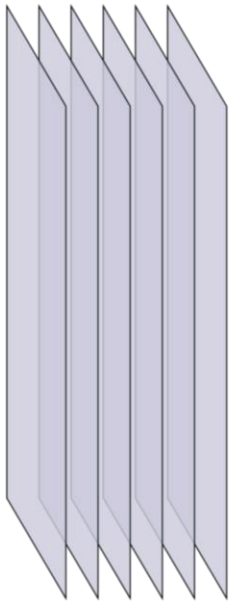

Incident field
$U_0(\mathbf{x})$

Refractive index of the medium (e.g., air)
n_0

Refractive index of object
$n(\mathbf{x})$

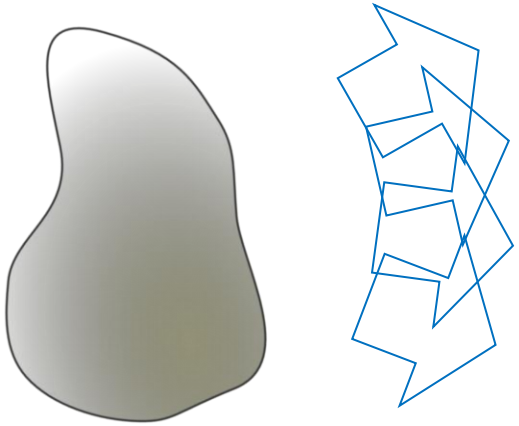

Object
$$O(\mathbf{x}) = k_0^2 \left[\left(\frac{n(\mathbf{x})}{n_0} \right)^2 - 1 \right]$$

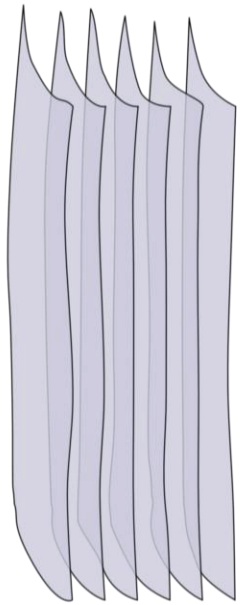

Total field (incident + scattered)
$U(\mathbf{x})$

Courtesy of the image: Paul Müller, Mirjam Schürmann, Jochen Guck, **The Theory of Diffraction Tomography**, available at: https://arxiv.org/pdf/1507.00466

Solution of the wave equation: general form

Inhomogeneous (scalar) wave equation

$$\underbrace{\left[\nabla^2 + k_0^2\right] U(\mathbf{x})}_{\text{Homogeneous term}} = \underbrace{-O(\mathbf{x})U(\mathbf{x})}_{\text{Forcing term}}$$

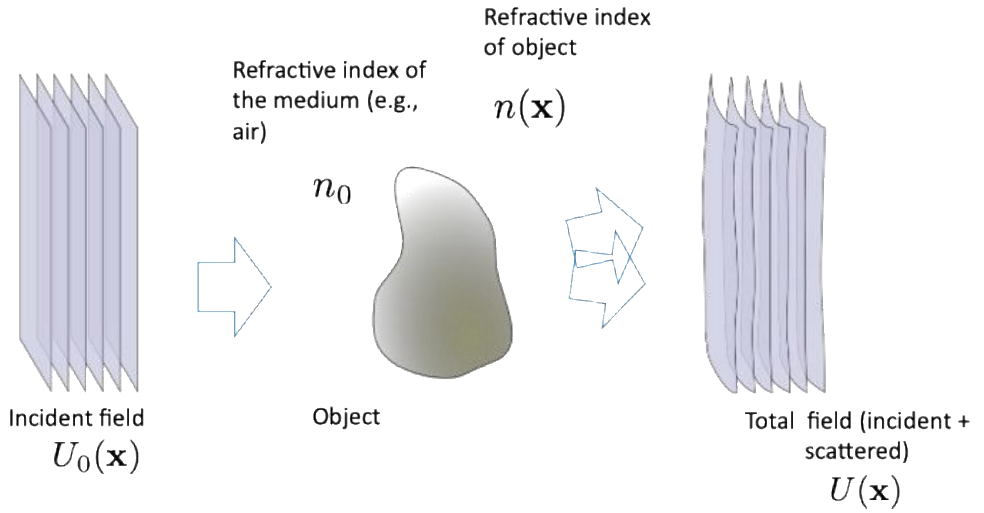

Object: the variation of the refractive index of the object w.r.t. surround medium

$$O(\mathbf{x}) = k_0^2 \left[\left(\frac{n(\mathbf{x})}{n_0} \right)^2 \right]$$

The scattered field is a function of **the field itself!**

Infinite reverberations of the incident field within the object

Solution of the inhomogeneous (scalar) wave equation (Lippm

$$U(\mathbf{x}) = \int G(\mathbf{x} - \mathbf{x}')O(\mathbf{x}')U(\mathbf{x}')\mathrm{d}^3\mathbf{x}'$$

$$G(\mathbf{x} - \mathbf{x}') = \frac{e^{-jk_0\|\mathbf{x}-\mathbf{x}'\|}}{4\pi\|\mathbf{x} - \mathbf{x}'\|}$$

Green function: 3D impulse response

The integral is over the object

Solution of the wave equation: Born approximation

Decompose the total field into incident and scattered

$$U(\mathbf{x}) = \underbrace{U_0(\mathbf{x})}_{\text{Incident wave}} + \underbrace{U_S(\mathbf{x})}_{\text{Scattered wave}}$$

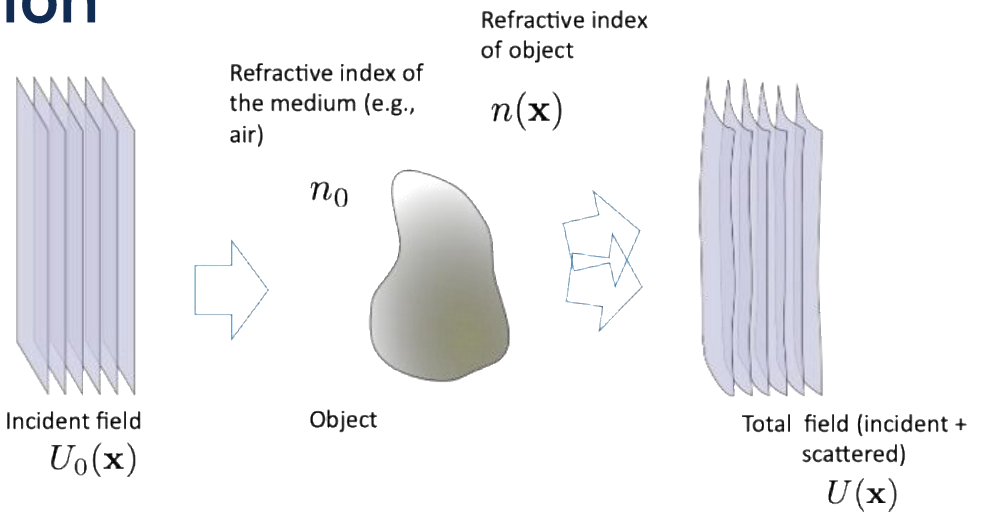

Weak scattering condition (Born approximation)

$|U_S(\mathbf{x})| \ll |U_0(\mathbf{x})|$ The scattered field is much weaker than the incident one

Approximated Lippmann-Schwinger integral equation

$$U(\mathbf{x}) \simeq U_0(\mathbf{x}) + \int G(\mathbf{x}-\mathbf{x}')O(\mathbf{x}')U_0(\mathbf{x}')\mathrm{d}^3\mathbf{x}'$$

Linear scattering theory: the scattered field is linear w.r.t. object

Plane wave approximation

Lippmann-Schwinger integral equation (Born approximation)

$$U(\mathbf{x}) \simeq U_0(\mathbf{x}) + \int G(\mathbf{x}-\mathbf{x}')O(\mathbf{x}')U_0(\mathbf{x}')\mathrm{d}^3\mathbf{x}'$$

Integral over the object volume

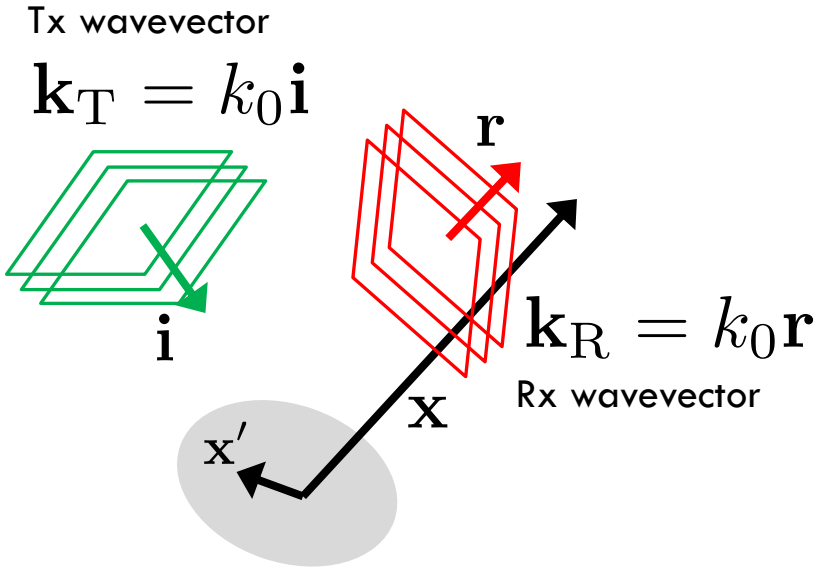

Let us consider far Tx and Rx

Fraunhofer approx of the Green function

Plane wave incident on the object

$$U_0(\mathbf{x}) = e^{-jk_0\mathbf{i}^T\mathbf{x}} \qquad G(\mathbf{x}-\mathbf{x}') \simeq \frac{e^{-jk_0(x-\mathbf{r}^T\mathbf{x}')}}{4\pi x}$$

The scattered field is written as:

3D Fourier transform of the object

$$U_S(\mathbf{x}) \simeq \int O(\mathbf{x}')e^{-jk_0(\mathbf{i}-\mathbf{r})^T\mathbf{x}'}\mathrm{d}^3\mathbf{x}'$$

The FT is evaluated in a single wavevector

$$\mathbf{k}^* = \mathbf{k}_\mathrm{T} - \mathbf{k}_\mathrm{R}$$

Ru Shan Wu and M. Nafi Toksz, (1987), "**Diffraction tomography and multisource holography applied to seismic imaging**," *GEOPHYSICS* 52: 11-25.

Scattered field as Fourier transform of the object function

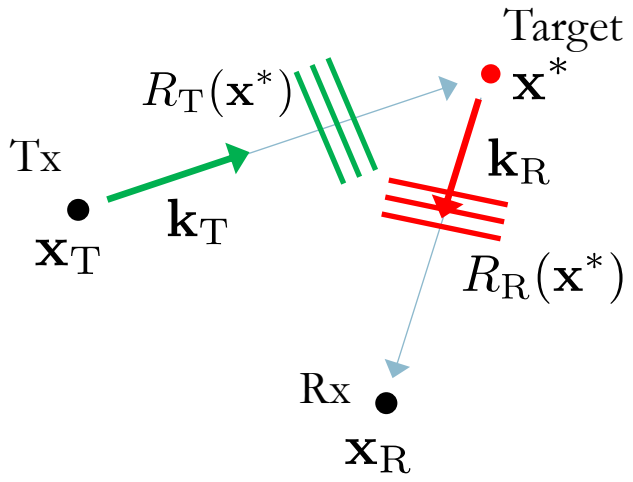

Diffraction tomography theorem:

- The response of a target to a collection of monochromatic plane waves is the Fourier transform of its spatial reflectivity function
- The more wavenumbers we illuminate, the finer is the spatial resolution

Caveat: if we process the signals *coherently*

$$U_S(\mathbf{x}) \simeq \int O(\mathbf{x}')e^{-j(\mathbf{k}_{\mathrm{T}}-\mathbf{k}_{\mathrm{R}})^T\mathbf{x}'}\mathrm{d}^3\mathbf{x}'$$

M. Manzoni, D. Tagliaferri, S. Tebaldini, M. Mizmizi, A. V. Monti-Guarnieri, C. M. Prati, and U. Spagnolini, **Wavefield networked sensing: Principles, algorithms, and applications**, IEEE Open Journal of the Communications Society, vol. 6, pp. 181–197, 2025.

Spatial ambiguity function (or point spreading function)

The image of a point target is defined as the Spatial Ambiguity Function (SAF)

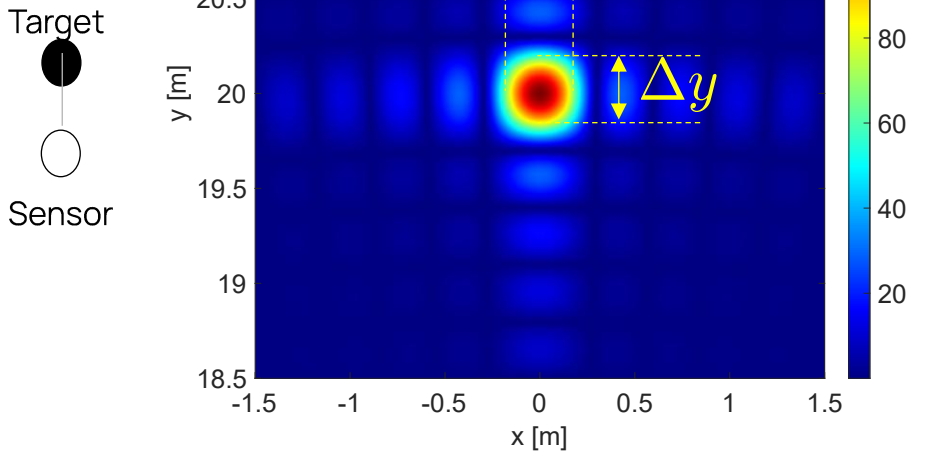

The **resolution** of the image is defined by the wavenumber set

$\mathcal{K}(B, A)$

With a finite **bandwidth** and a finite **aperture,** we can cover (i.e., sample) a wavenumber **set**

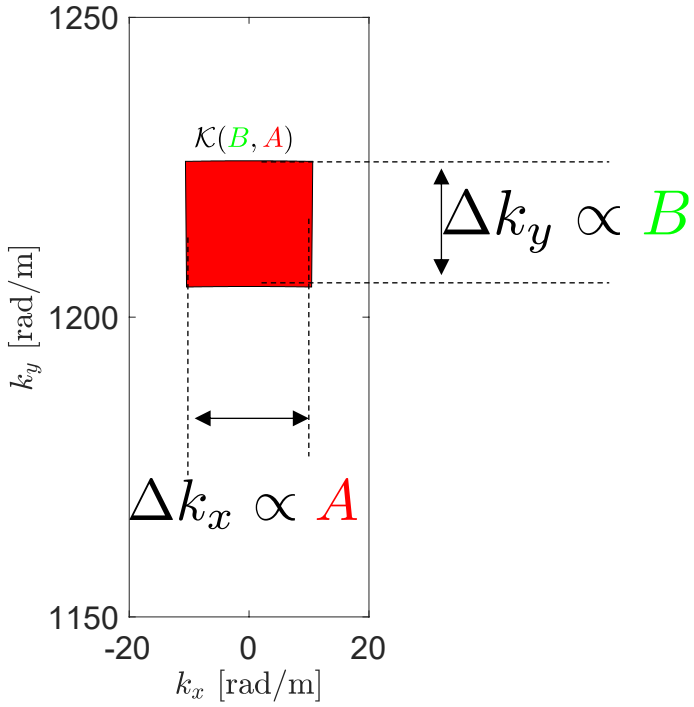

$$\Delta x = \frac{2\pi}{\Delta k_x}$$

$$\Delta y = \frac{2\pi}{\Delta k_y}$$

The SAF is the building block of any image (*obtained with linear approaches*)

Outline

1. **Radio imaging in ISAC systems**
   - Brief recall of fundamentals
   - Methods (linear and non-linear)

Image formation in OFDM-based ISAC systems

Tx OFDM baseband signal (with BF)

$$\mathbf{g}(t) = \mathbf{f} \underbrace{\sum_{m\in\mathcal{M}} s_m e^{j2\pi m\Delta f t} \mathrm{rect}\left(\frac{t}{T}\right)}_{g(t)}$$

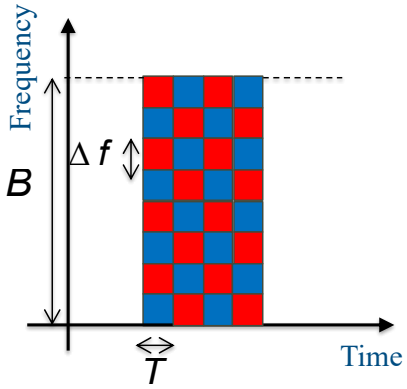

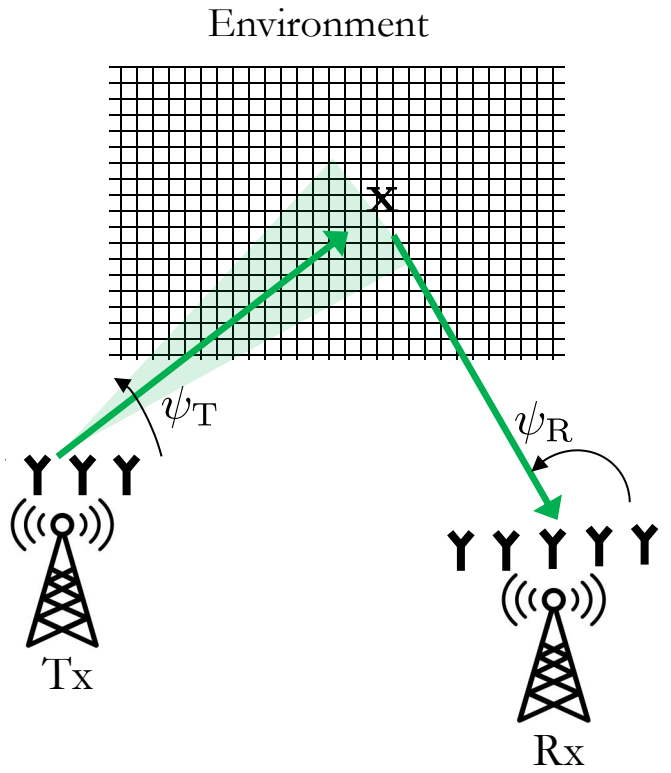

Rx OFDM signal (perfect sync, after demodulation)

Integral over the environment

Array response (Rx)

Array response (Tx)

Propagation phase

$$\mathbf{y}(t) = \sqrt{P} \iint \rho(\mathbf{x})\gamma(\mathbf{x})\mathbf{a}(\psi_{\mathrm{R}}(\mathbf{x}))\mathbf{a}^{\top}(\psi_{\mathrm{T}}(\mathbf{x}))\mathbf{g}(t-\tau(\mathbf{x}))e^{-j2\pi f_0\tau(\mathbf{x})}d\mathbf{x} + \mathbf{w}(t)$$

Noise

General model

Path loss component

$$\rho(\mathbf{x}) = \frac{\lambda_0}{(4\pi)^{3/2}\|\mathbf{x}-\mathbf{x}_{\mathrm{T}}\|\|\mathbf{x}-\mathbf{x}_{\mathrm{R}}\|}$$

Complex reflectivity

$$\gamma(\mathbf{x}) = \sqrt{\Gamma(\mathbf{x})}e^{j\phi(\mathbf{x})}$$

Time of flight (TOF)

$$\tau(\mathbf{x}) = \frac{\|\mathbf{x}-\mathbf{x}_{\mathrm{T}}\| + \|\mathbf{x}-\mathbf{x}_{\mathrm{R}}\|}{c}$$

CFR reconstruction

Tx OFDM baseband signal (with BF)

$$\mathbf{g}(t) = \mathbf{f} \underbrace{\sum_{m \in \mathcal{M}} s_m e^{j2\pi m \Delta f t} \mathrm{rect}\left(\frac{t}{T}\right)}_{g(t)}$$

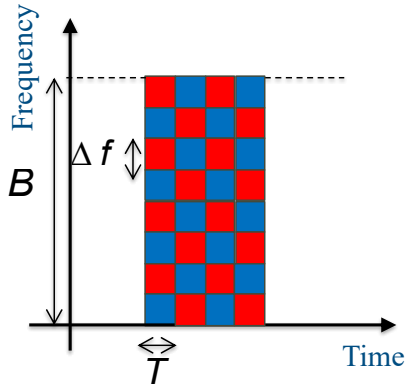

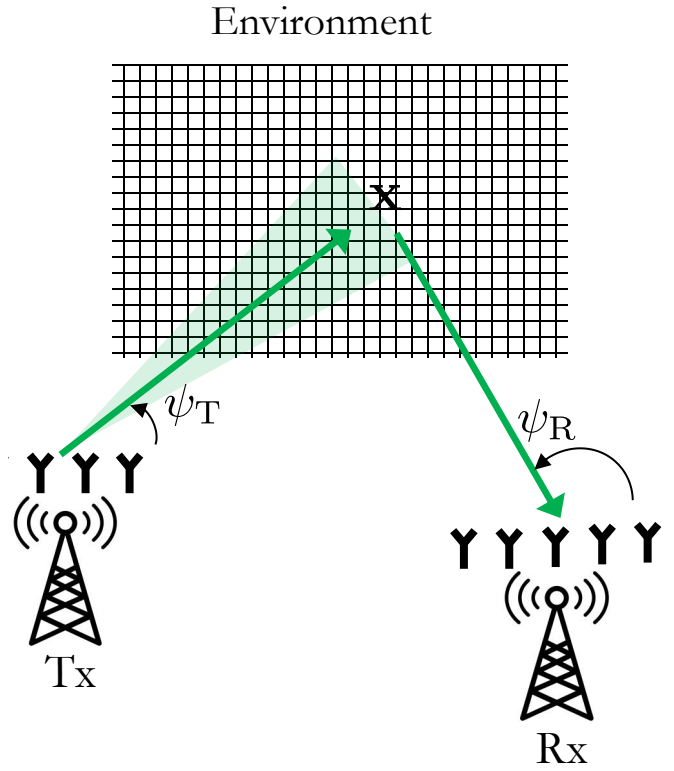

1) Frequency domain and sampling at subcarrier location

$$\boldsymbol{y}(m\Delta f) = \sqrt{P} s_m \iint \tilde{\rho}(\mathbf{x}) \mathbf{a}(\psi_R(\mathbf{x})) e^{-j2\pi(f_0 + m\Delta f)\tau(\mathbf{x})} \gamma(\mathbf{x}) d\mathbf{x} + \boldsymbol{w}(m\Delta f)$$

2) Obtain the channel frequency response (CFR) at the m-th subcarrier

$$\boldsymbol{h}(m\Delta f) = \iint \tilde{\rho}(\mathbf{x}) \mathbf{a}(\psi_R(\mathbf{x})) e^{-j2\pi(f_0 + m\Delta f)\tau(\mathbf{x})} \gamma(\mathbf{x}) d\mathbf{x} + \boldsymbol{n}(m\Delta f)$$

2.1) Compute the CFR at pilot location (using LS/MMSE techniques)
2.2) Interpolate to obtain the CFR on any subcarrier

Approximation of the CFR and imaging problem

3) Approximation of the CFR

$$\boldsymbol{h}(m\Delta f) = \iint \tilde{\rho}(\mathbf{x})\mathbf{a}(\psi_{\mathrm{R}}(\mathbf{x}))e^{-j2\pi(f_0+m\Delta f)\tau(\mathbf{x})}\gamma(\mathbf{x})d\mathbf{x} + \boldsymbol{n}(m\Delta f)$$

$$\approx \sum \tilde{\rho}(\mathbf{x})\mathbf{a}(\psi_{\mathrm{R}}(\mathbf{x}))e^{-j2\pi(f_0+m\Delta f)\tau(\mathbf{x})}\gamma(\mathbf{x}) + \boldsymbol{n}(m\Delta f)$$ Grid of pixels

$$= \boldsymbol{B}(m\Delta f)\,\boldsymbol{\gamma} + \boldsymbol{n}(m\Delta f)$$ Linear system w.r.t. reflectivity (through the **sensing matrix *B***) → A column of ***B*** represents the Rx signal at the Rx antennas due to the scattering from a pixel

$$\tilde{\boldsymbol{h}} = [\boldsymbol{h}^{\top}(\Delta f), \ldots, \boldsymbol{h}^{\top}(M\Delta f)]^{\top}$$

$$= \begin{bmatrix} \sum \tilde{\rho}(\mathbf{x})\mathbf{a}(\psi_{\mathrm{R}}(\mathbf{x}))e^{-j2\pi(f_0+\Delta f)\tau(\mathbf{x})} \\ \vdots \\ \sum \tilde{\rho}(\mathbf{x})\mathbf{a}(\psi_{\mathrm{R}}(\mathbf{x}))e^{-j2\pi(f_0+M\Delta f)\tau(\mathbf{x})} \end{bmatrix} \gamma(\mathbf{x}) + \tilde{\boldsymbol{n}} = \tilde{\boldsymbol{B}}\boldsymbol{\gamma} + \tilde{\boldsymbol{n}}$$ Stacking all data

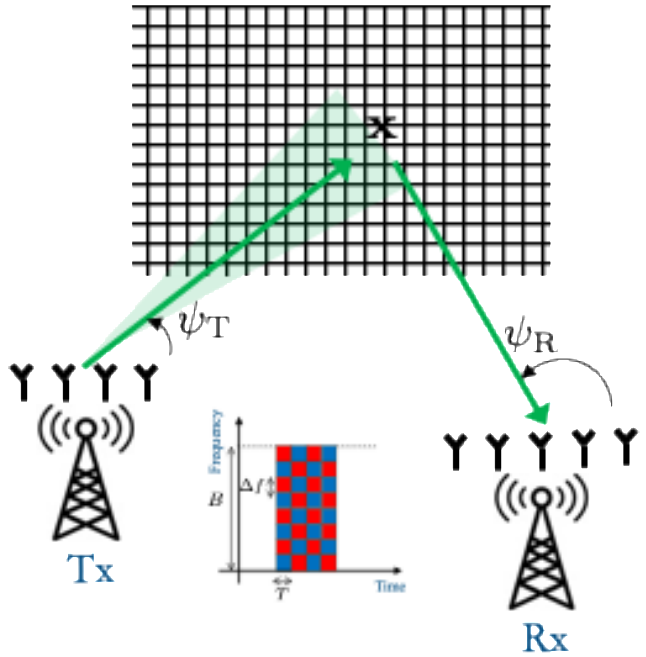

Considerations:

3.1) Estimate the reflectivity over a continuous set is not possible,
→ We need an appropriate **pixel-wise representation** of the reflectivity

3.2) We have M subcarriers and L antennas, and *much more* (typically) pixels
→ The **direct inversion of the linear problem is (generally) not possible**

Image formation by matched filter

4) Image formation by **matched filter** (***back-projection***)

$$\widetilde{\boldsymbol{h}} = \widetilde{\boldsymbol{B}}\boldsymbol{\gamma} + \widetilde{\boldsymbol{n}}$$

$$\widehat{\boldsymbol{\gamma}} = \widetilde{\boldsymbol{B}}^{\mathrm{H}}\widetilde{\boldsymbol{h}} = \widetilde{\boldsymbol{B}}^{\mathrm{H}}\widetilde{\boldsymbol{B}}\boldsymbol{\gamma} + \widetilde{\boldsymbol{B}}^{\mathrm{H}}\widetilde{\boldsymbol{n}}$$

Image as the estimation of the reflectivity

Compensation for the path-loss

Compensation for the propagation phase

Rx BF for pixel x

$$I(\mathbf{x}) = \widehat{\gamma}(\mathbf{x}) = \frac{1}{\widetilde{\rho}(\mathbf{x})} \sum_{m \in \mathcal{M}} e^{j2\pi(f_0 + m\Delta f)\tau(\mathbf{x})} \mathbf{a}^{\mathrm{H}}(\psi_{\mathrm{R}}(\mathbf{x}))\boldsymbol{h}(m\Delta f)$$

$$\simeq \gamma(\mathbf{x}) * *\chi(\mathbf{x}) + Z(\mathbf{x})$$

Spatial noise

Spatial ambiguity function (SAF)

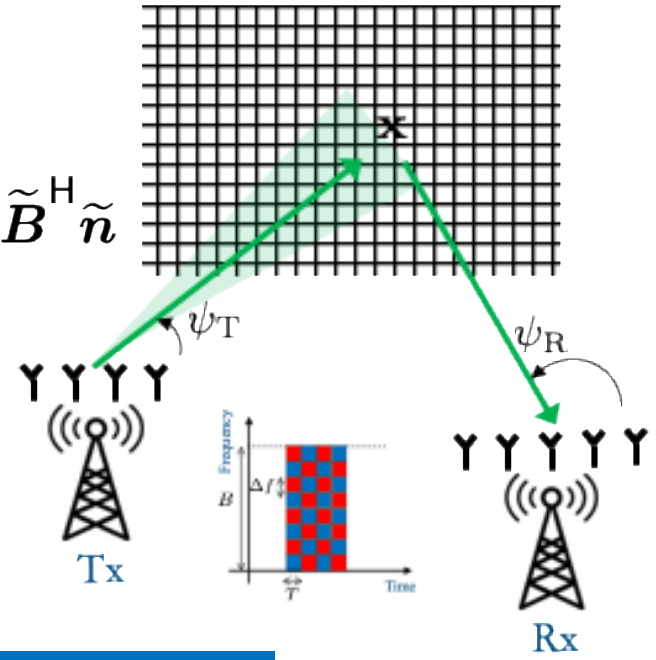

The MF provides the estimation of the reflectiviy but **blurred** by the SAF

Remarks:

4.1) The effective imaging capabilities for linear techniques (MF) are ruled by SAF
→ resolution and sidelobe levels

4.2) Any trick to augment the measurements (e.g., increasing the samples in frequency) does not improve the result: imaging is ruled by SAF

4.3) If **prior information** is available on the environment (e.g., sparsity)
→ **non-linear techniques** may perform better than MF

L. C. Potter, E. Ertin, J. T. Parker, and M. Cetin, "**Sparsity and compressed sensing in radar imaging**," Proceedings of the IEEE, vol. 98, no. 6, pp. 1006–1020, 2010

J. Yang, T. Jin, C. Xiao, and X. Huang, "**Compressed sensing radar imaging: Fundamentals, challenges, and advances**," Sensors, vol. 19, no. 14, 2019. [Online]. Available: https://www.mdpi.com/1424-8220/19/14/3100

Non-linear Image formation (hints)

Object

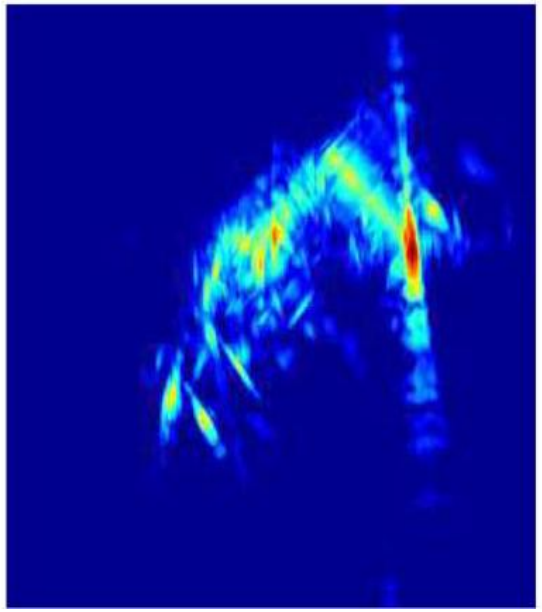

MF image

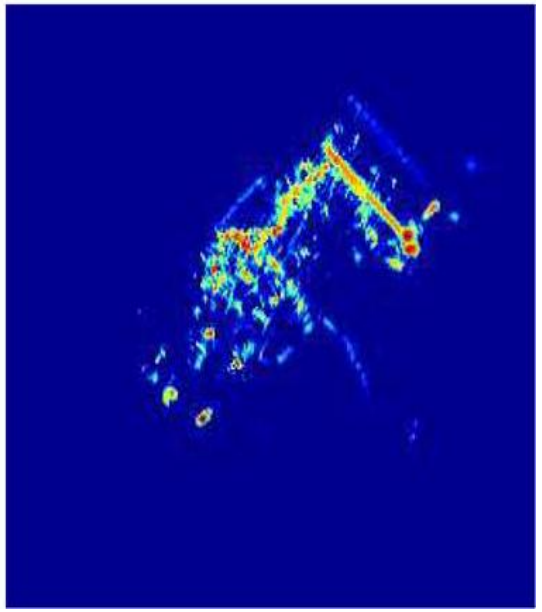

CS image

Image courtesy from L.C. Potter et al

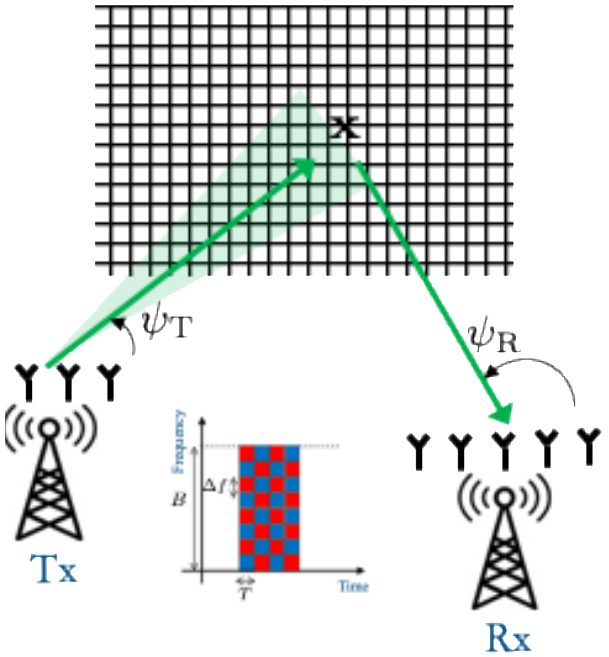

L. C. Potter, E. Ertin, J. T. Parker, and M. Cetin, "**Sparsity and compressed sensing in radar imaging**," Proceedings of the IEEE, vol. 98, no. 6, pp. 1006–1020, 2010

J. Yang, T. Jin, C. Xiao, and X. Huang, "**Compressed sensing radar imaging: Fundamentals, challenges, and advances**," Sensors, vol. 19, no. 14, 2019. [Online]. Available: https://www.mdpi.com/1424-8220/19/14/3100

Outline

1. **Radio imaging in ISAC systems**
   - Brief recall of fundamentals
   - Methods (linear and non-linear)
   - Coherent multistatic imaging and integration into ISAC

Multistatic imaging

How to fuse the images in an ISAC network?

Incoherent (baseband) fusion: images are summed by retaining the **amplitude information** only

Coherent (pass-band) fusion: images are summed by retaining the **amplitude and carrier phase information**

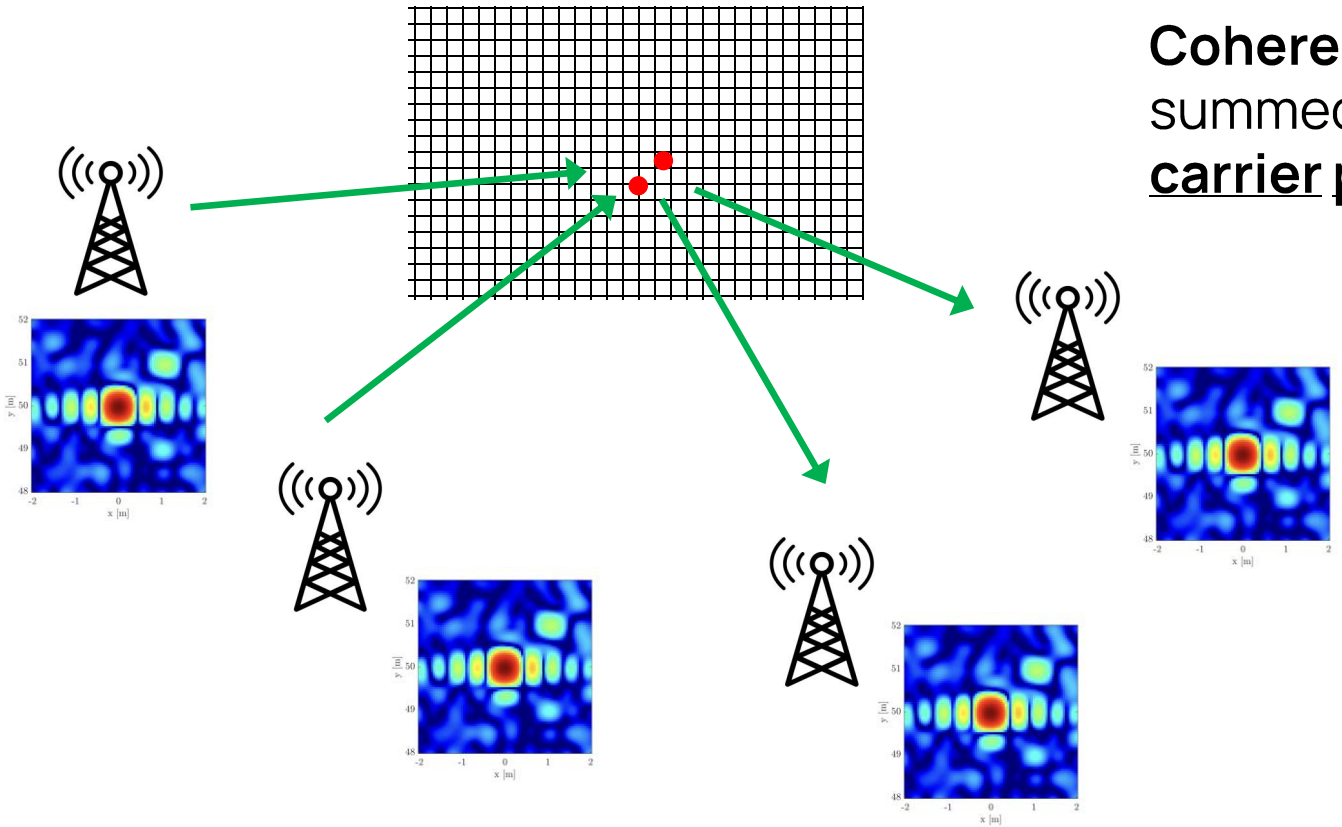

Only coherent fusion enhances resolution!

The importance of bistatic data: insight from a toy example

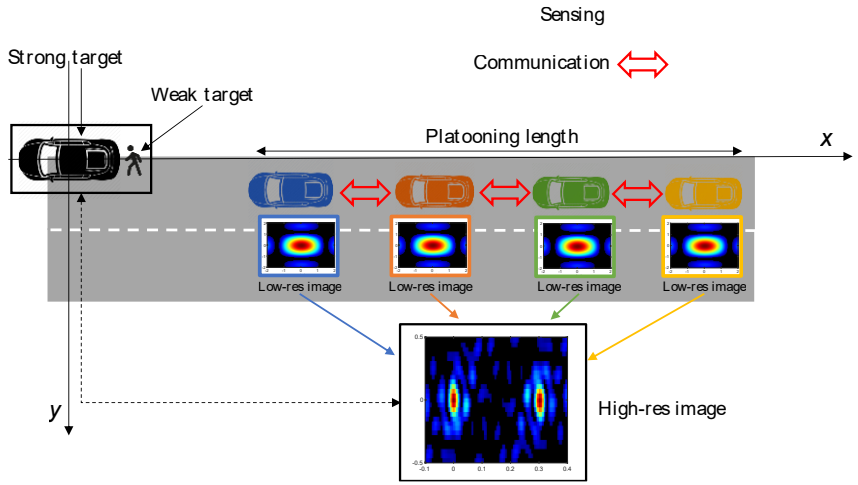

Use case: weak target detection in clutter (nearby to a stronger one) such as a pedestrian close to a parker car for automotive applications

Spatial frequencies illuminated by the vehicles

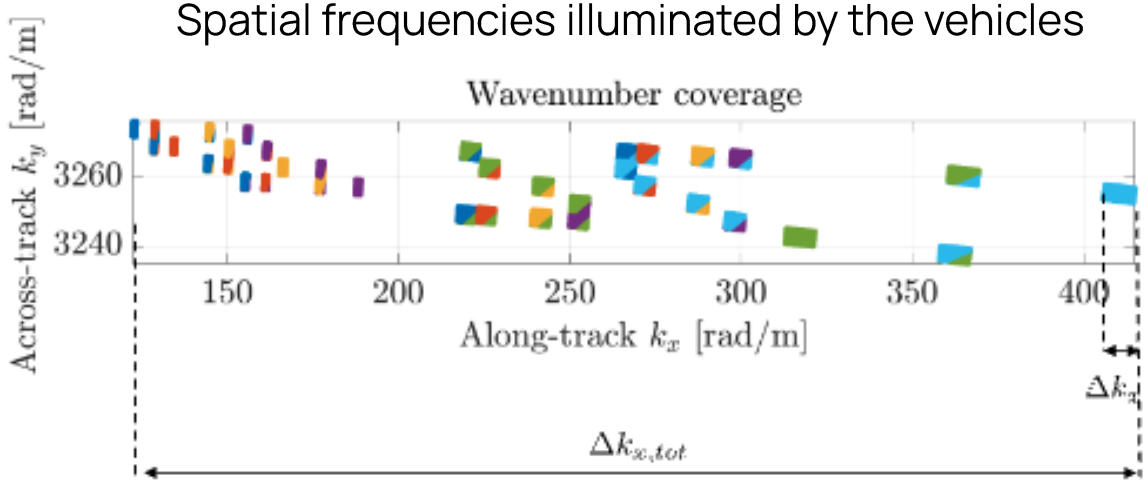

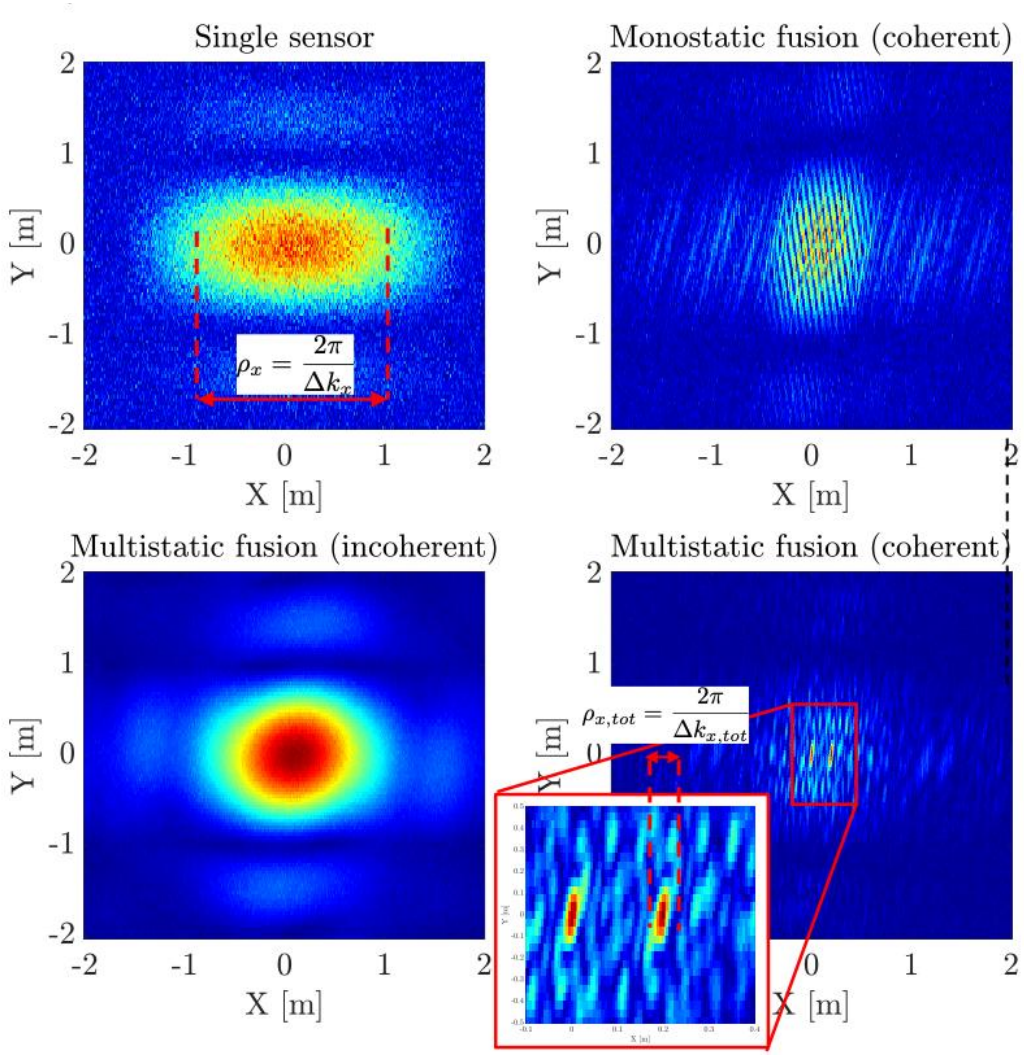

An experimental example in the 77 GHz automotive scenario

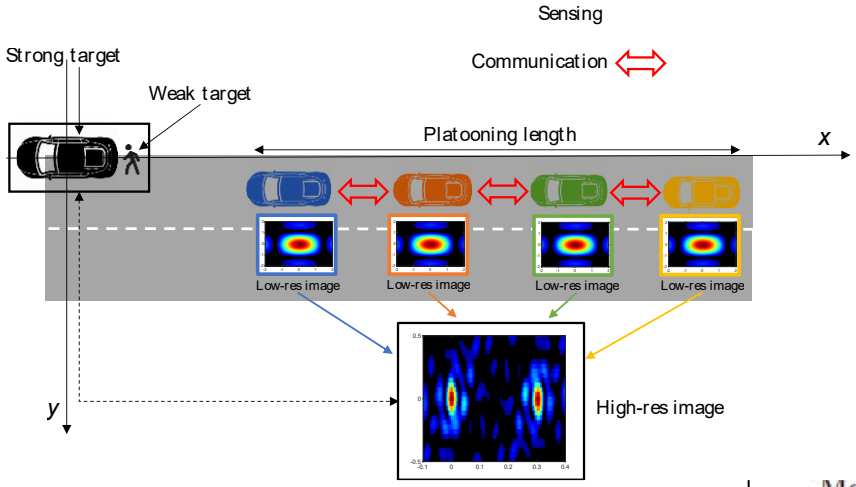

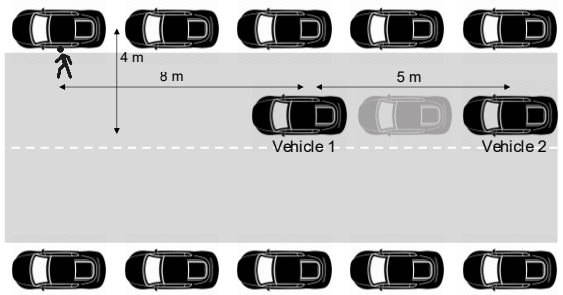

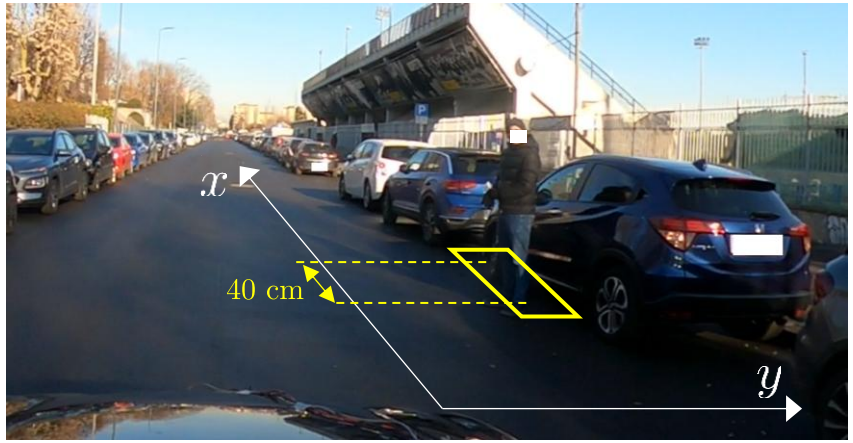

The experimental verification of the previous example (with 2 cars)

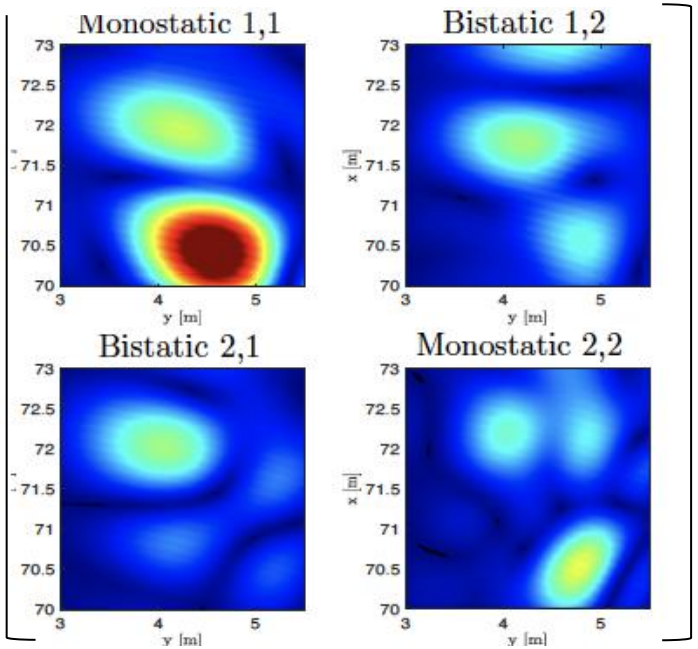

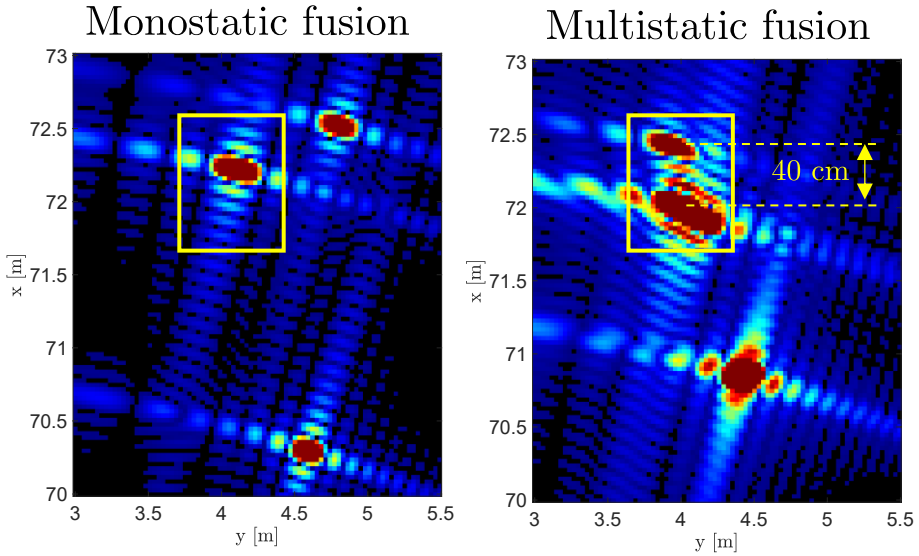

We can see the legs of the pedestrian

D. Tagliaferri *et al.*, "**Cooperative Coherent Multistatic Imaging and Phase Synchronization in Networked Sensing**," in *IEEE Journal on Selected Areas in Communications*, vol. 42, no. 10, pp. 2905-2921, Oct. 2024, doi: 10.1109/JSAC.2024.3414609

Imaging in D-MIMO networks: integration challenges

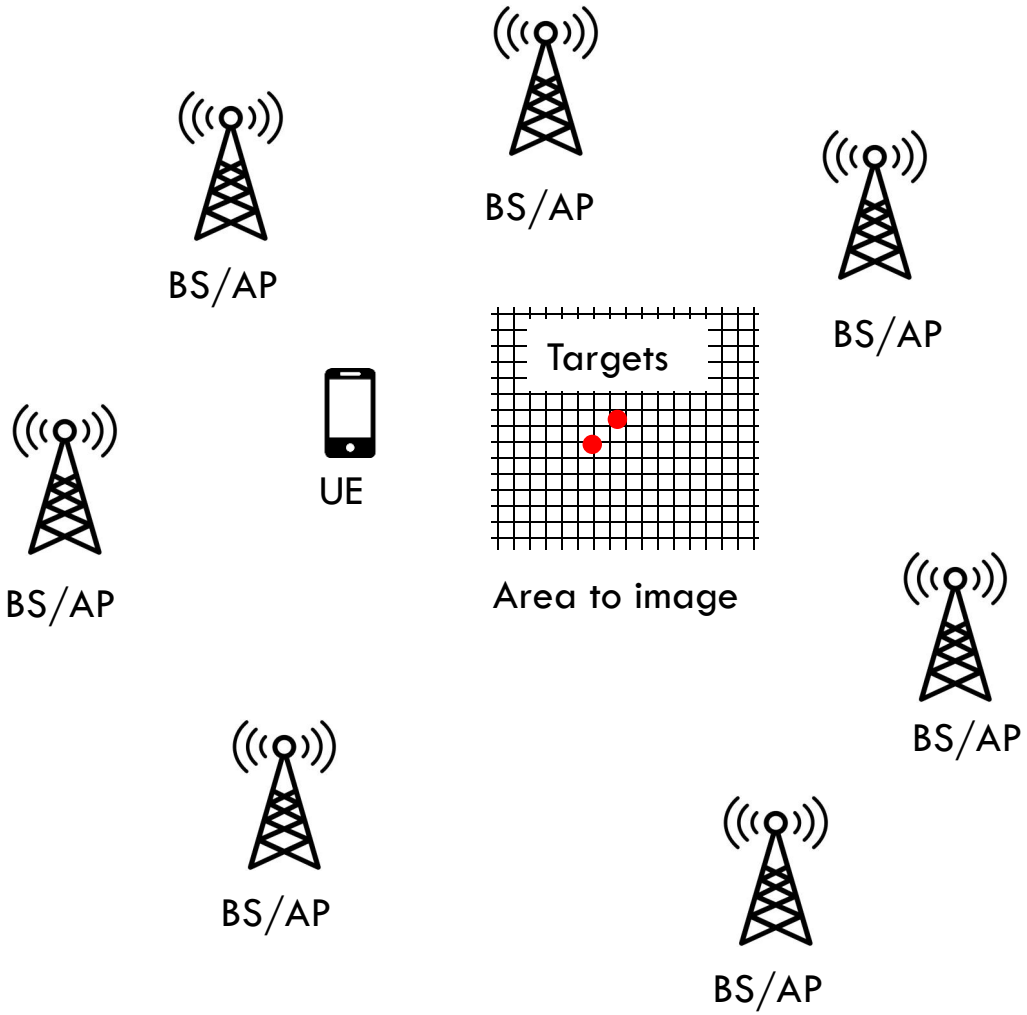

- Downlink systems
  - Typical **half-duplex** AP operation (depends on setup) → All AP are Tx (**no Rx for multistatic imaging**)

D. Tagliaferri, S. Mura, M.F. Keskin, S. Dey, H. Wymeersch, «**Integrating Phase-Coherent Multistatic Imaging in Downlink D-MIMO Networks**», https://arxiv.org/pdf/2510.04240

Imaging in D-MIMO networks: integration challenges

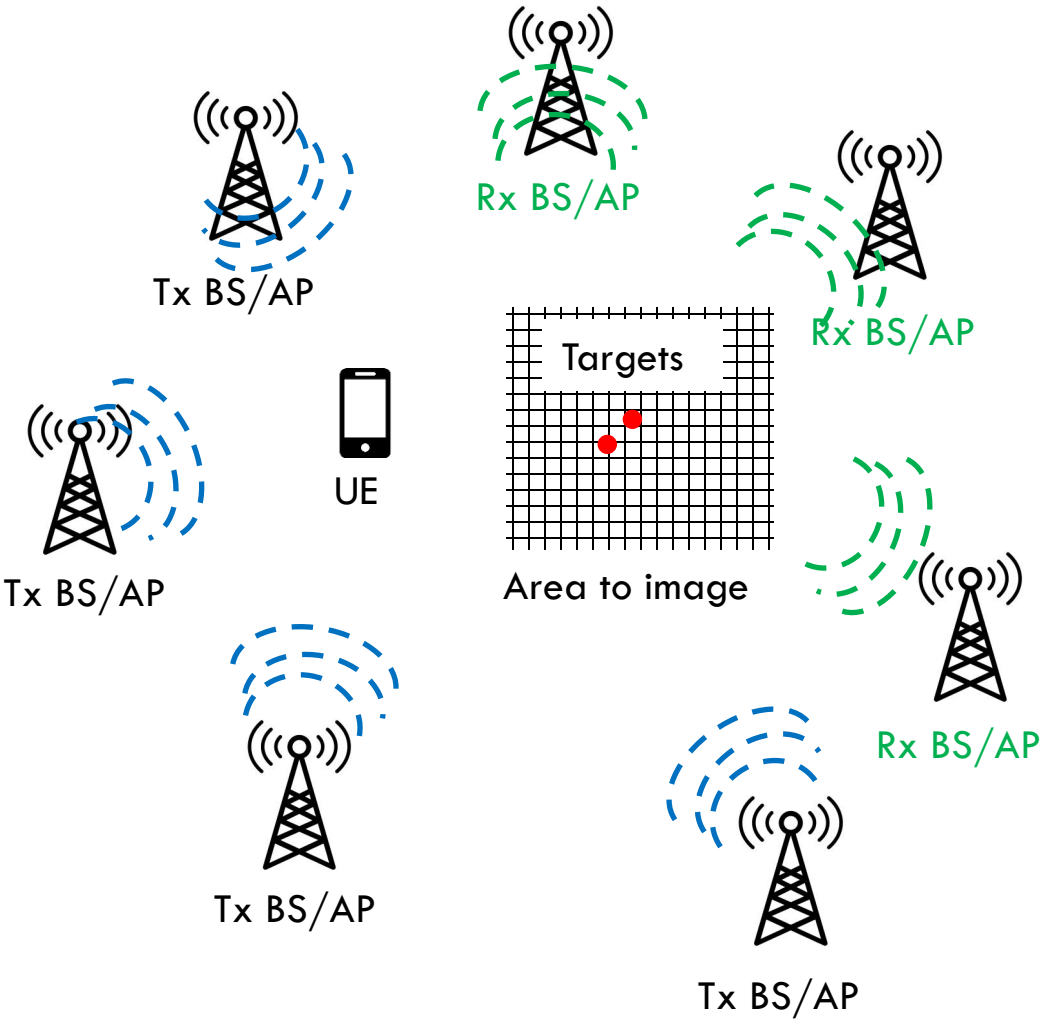

- Downlink systems
  - Typical **half-duplex** AP operation (depends on setup) → All AP are Tx (**no Rx for multistatic imaging**)
  - ✓ Possible strategy: devise an optimal Tx-Rx AP mode selection

D. Tagliaferri, S. Mura, M.F. Keskin, S. Dey, H. Wymeersch, «**Integrating Phase-Coherent Multistatic Imaging in Downlink D-MIMO Networks**», https://arxiv.org/pdf/2510.04240

Imaging in D-MIMO networks: integration challenges

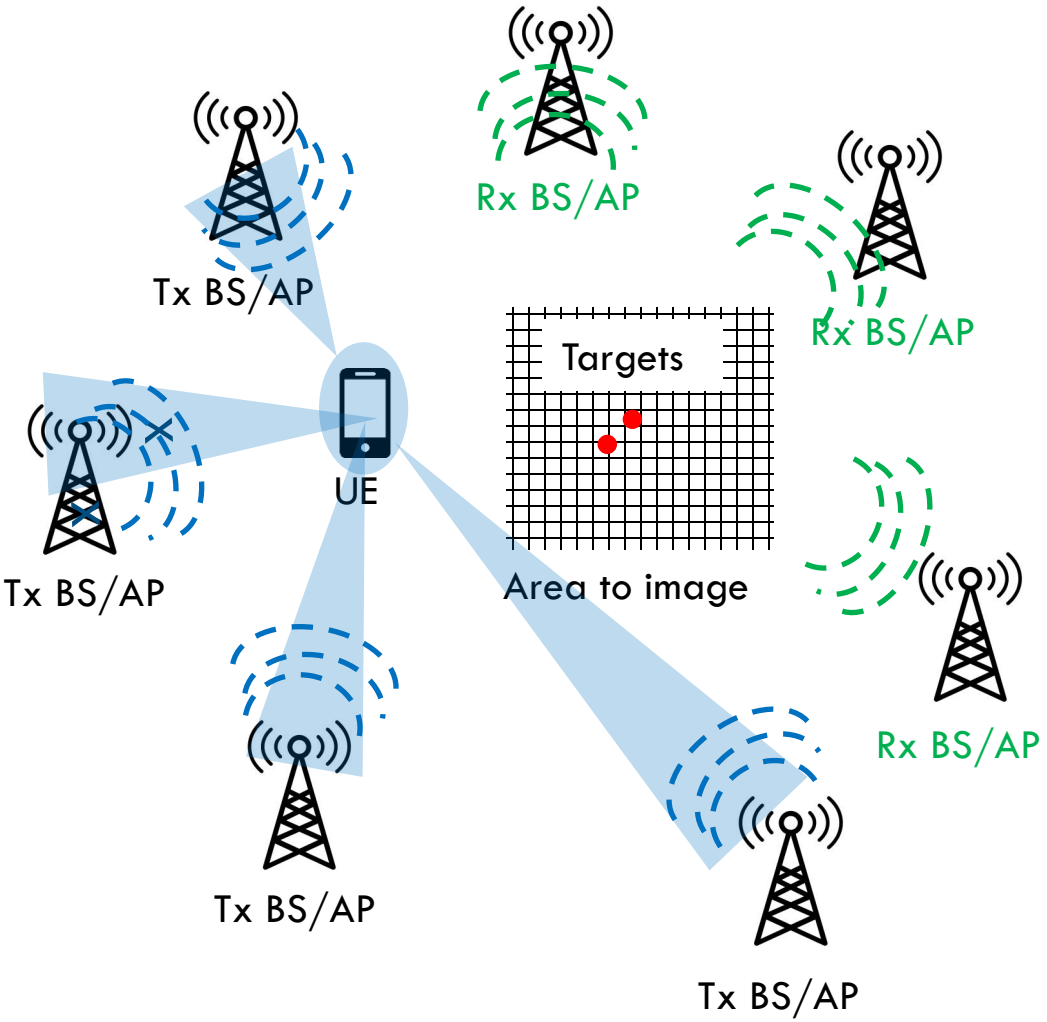

- Downlink systems
  - Typical **half-duplex** AP operation (depends on setup) → All AP are Tx (**no Rx for multistatic imaging**)
  - Tx AP employ **spatial precoding** to focus the signal at the UE (maximizing the capacity) → **no illumination of the area** to be imaged

D. Tagliaferri, S. Mura, M.F. Keskin, S. Dey, H. Wymeersch, «**Integrating Phase-Coherent Multistatic Imaging in Downlink D-MIMO Networks**», https://arxiv.org/pdf/2510.04240

Imaging in D-MIMO networks: integration challenges

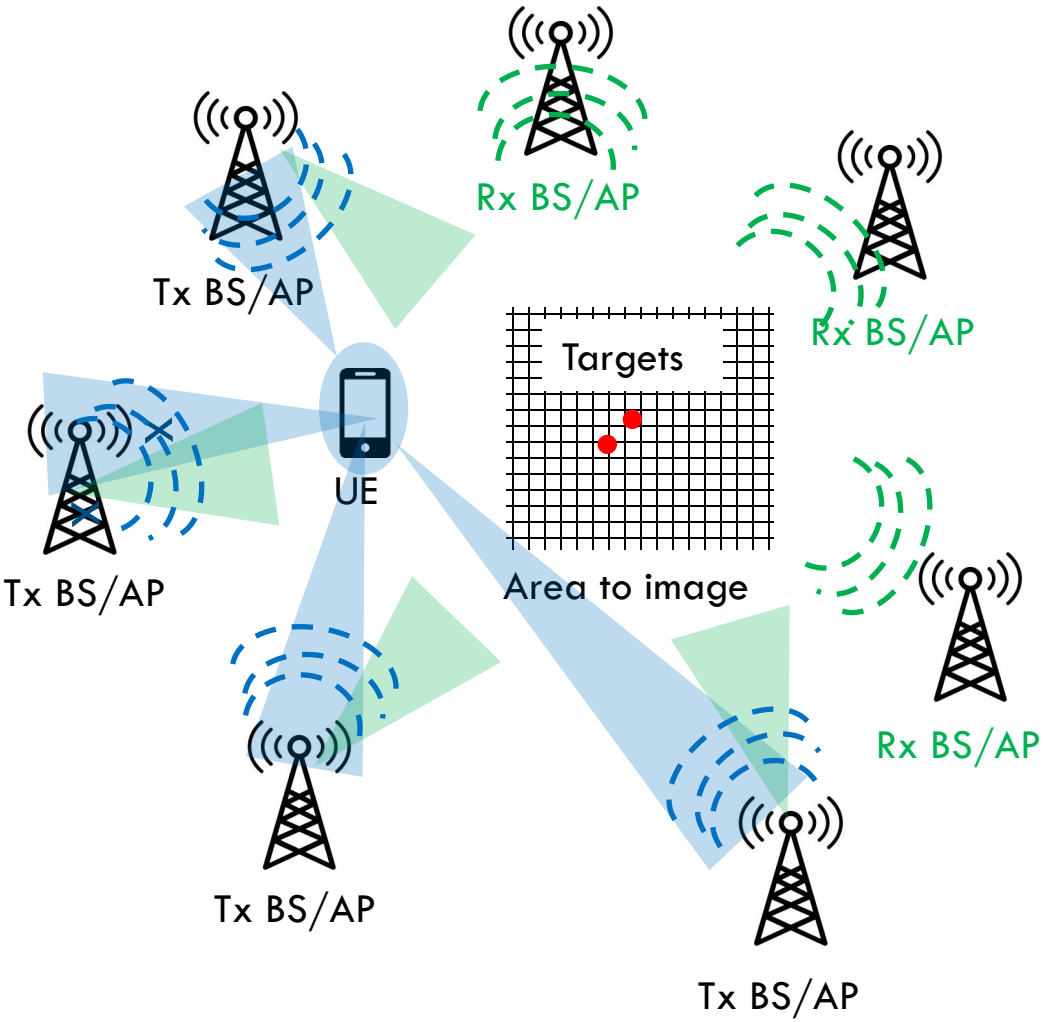

- Downlink systems
  - Typical **half-duplex** AP operation (depends on setup) → All AP are Tx (**no Rx for multistatic imaging**)
  - Tx AP employ **spatial precoding** to focus the signal at the UE (maximizing the capacity) → **no illumination of the area** to be imaged
  - ✓ Possible strategy: envision a dedicated ISAC precoding

D. Tagliaferri, S. Mura, M.F. Keskin, S. Dey, H. Wymeersch, «**Integrating Phase-Coherent Multistatic Imaging in Downlink D-MIMO Networks**», https://arxiv.org/pdf/2510.04240

Imaging in D-MIMO networks: integration challenges

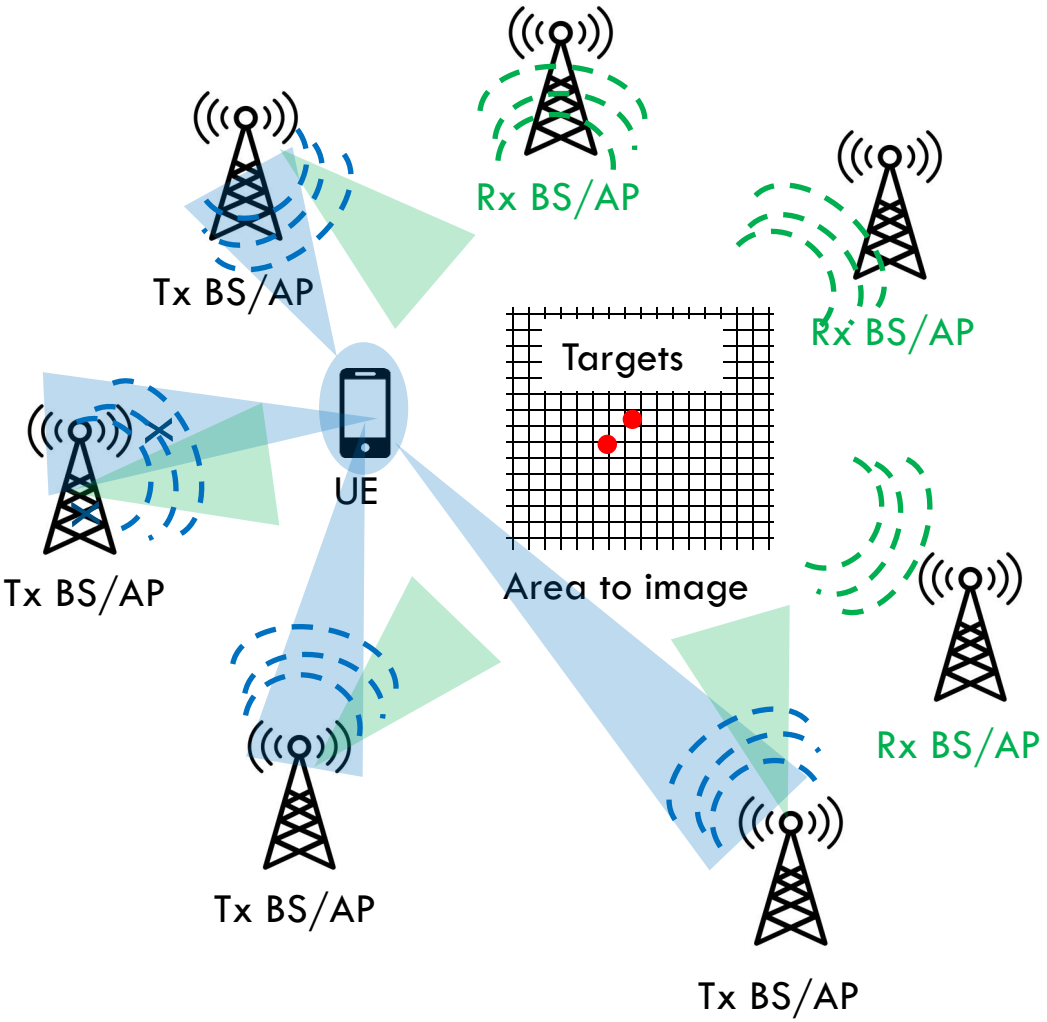

- Downlink systems
  - Typical **half-duplex** AP operation (depends on setup) → All AP are Tx (**no Rx for multistatic imaging**)
  - Tx AP employ **spatial precoding** to focus the signal at the UE (maximizing the capacity) → **no illumination of the area** to be imaged
  - Tx AP emit **the same signal in time and frequency**
  - ✓ Possible strategy: envision a smart communication-imaging signal coexistence

Imaging calls for orthogonal signaling among Tx, vice-versa for communication

D. Tagliaferri, S. Mura, M.F. Keskin, S. Dey, H. Wymeersch, «**Integrating Phase-Coherent Multistatic Imaging in Downlink D-MIMO Networks**», https://arxiv.org/pdf/2510.04240

Imaging in D-MIMO networks: integration challenges

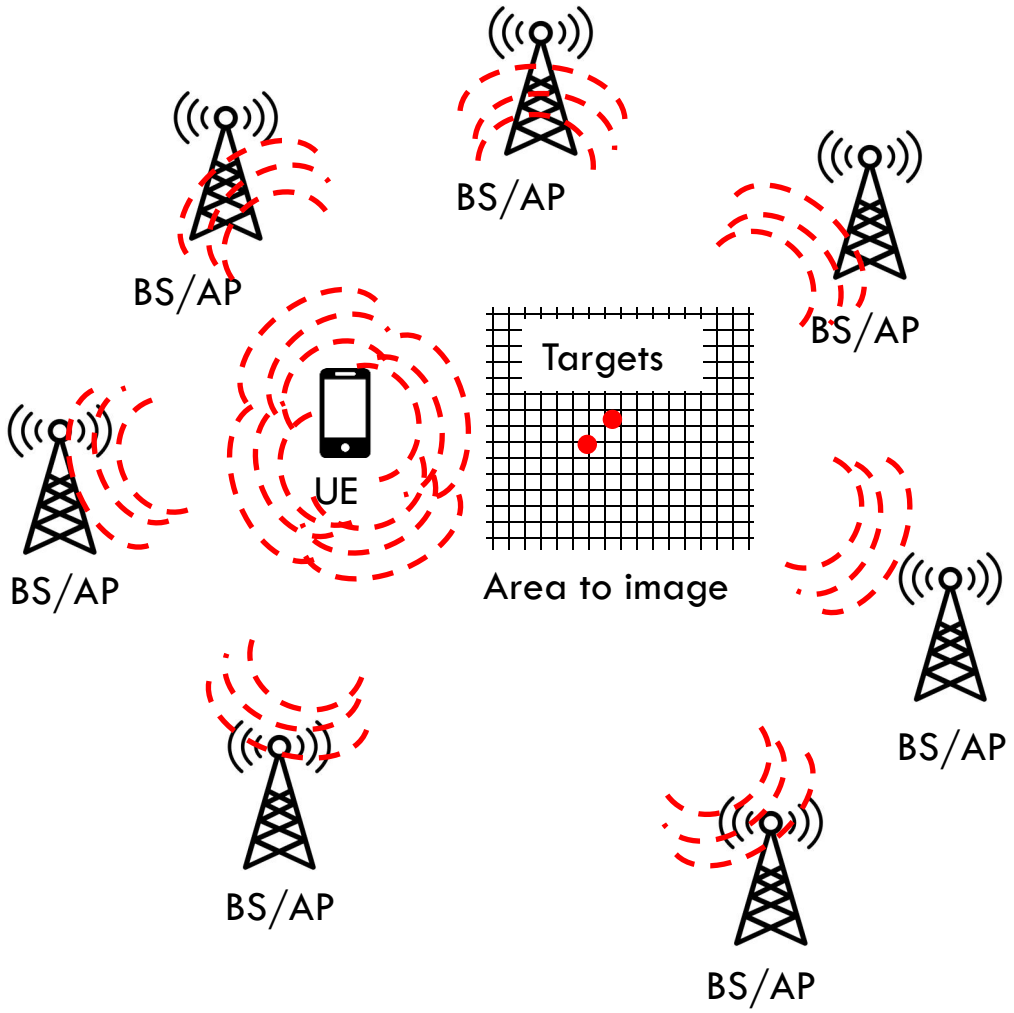

- Downlink systems
  - Typical **half-duplex** AP operation (depends on setup) → All AP are Tx (**no Rx for multistatic imaging**)
  - Tx AP employ **spatial precoding** to focus the signal at the UE (maximizing the capacity) → **no illumination of the area** to be imaged
  - Tx AP emit **the same signal in time and frequency**
- Uplink systems
  - Clock mismatch between UE and AP, unknown position of the UE → **need for synchronization and phase calibration**

Imaging in D-MIMO networks: integration challenges

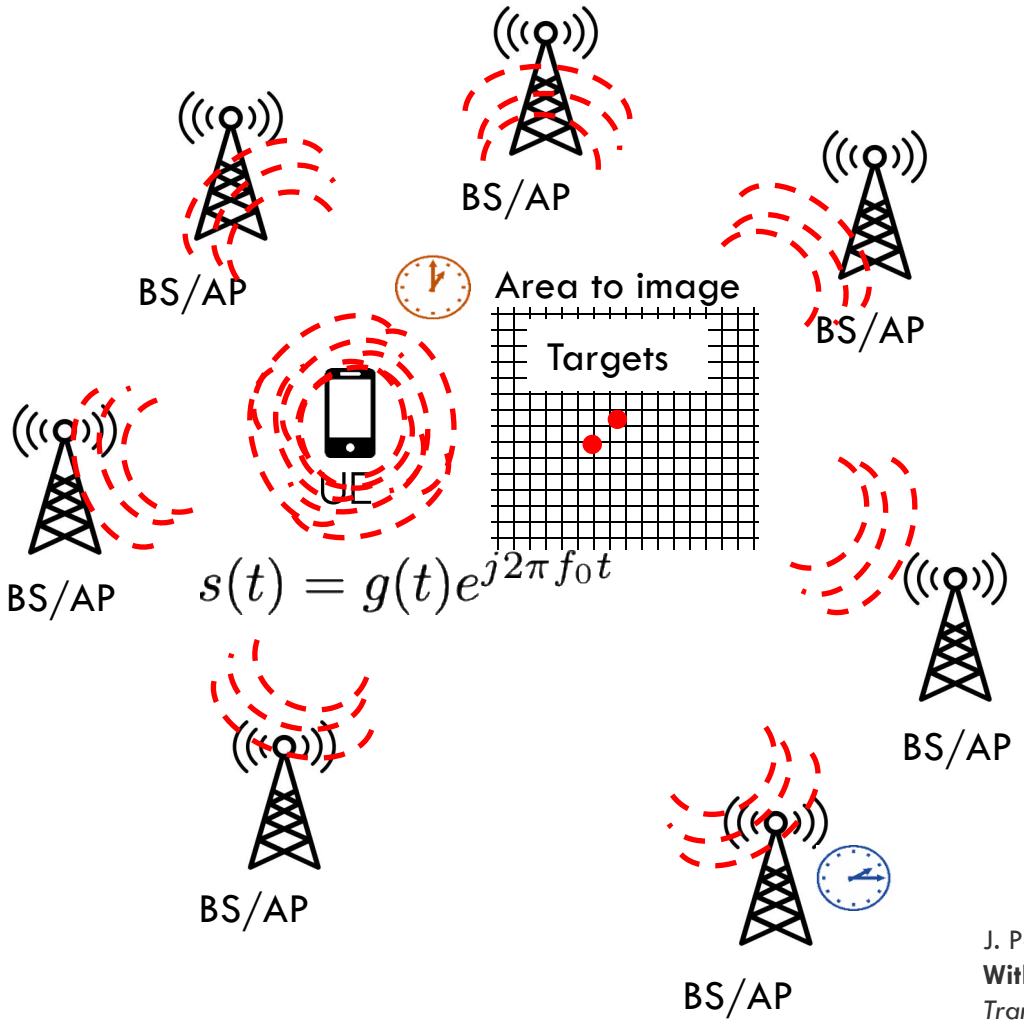

- Downlink systems
  - Typical **half-duplex** AP operation (depends on setup) → All AP are Tx (**no Rx for multistatic imaging**)
  - Tx AP employ **spatial precoding** to focus the signal at the UE (maximizing the capacity) → **no illumination of the area** to be imaged
  - Tx AP emit **the same signal in time and frequency**
- Uplink systems
  - Clock mismatch between UE and AP, unknown position of the UE → **need for synchronization and phase calibration**

UE time error at the time of Rx

AP time error at the time of Rx

$$y_n(t) = s(t - \tau_n + \varepsilon(t - \tau_n) - \epsilon_n(t)) + w_n(t)$$

J. Pegoraro *et al.*, "**JUMP: Joint Communication and Sensing With Unsynchronized Transceivers Made Practical**," in *IEEE Transactions on Wireless Communications*, vol. 23, no. 8, pp. 9759-9775, Aug. 2024, doi: 10.1109/TWC.2024.3365853

D. Tagliaferri *et al.*, "**Cooperative Coherent Multistatic Imaging and Phase Synchronization in Networked Sensing**," in *IEEE Journal on Selected Areas in Communications*, vol. 42, no. 10, pp. 2905-2921, Oct. 2024, doi: 10.1109/JSAC.2024.3414609

Outline

1. **Radio imaging in ISAC systems**
   - Brief recall of fundamentals
   - Methods (linear and non-linear)
   - Coherent multistatic imaging and integration into ISAC

2. **Multi-band sensing at FR3**
   - Motivation, potential and challenges

The opportunity: FR3 spectrum

- ✓ **6G** is expected use the **FR3** (roughly **6 GHz to 24 GHz**) for wireless communications (mobile radio networks), as they balance coverage and available bandwidth

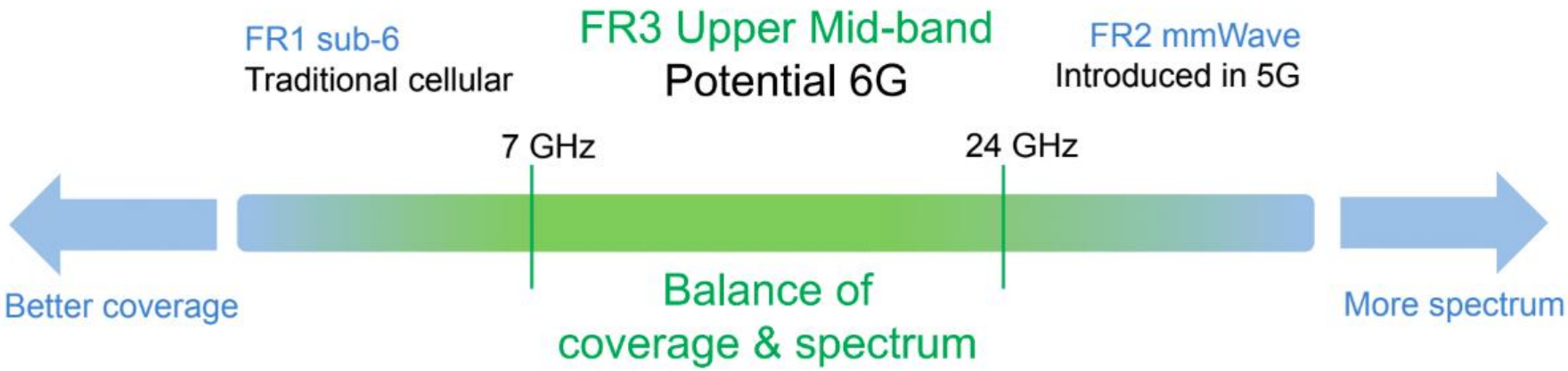

Challenges with FR3

- ❑ Wide spectrum
- ❑ Incumbents
- ❑ Need for robustness
- ❑ Fast reconfigurability

FR3 experimental platforms are needed!

Image courtesy from: S. Kang *et al.*, "**Cellular Wireless Networks in the Upper Mid-Band**," in *IEEE Open Journal of the Communications Society*, vol. 5, pp. 2058-2075, 2024, doi: 10.1109/OJCOMS.2024.3373368

The opportunity: different spectrum portions

- ✓ **6G** is expected use the **FR3** (roughly **6 GHz to 24 GHz**) for wireless communications (mobile radio networks), as they balance coverage and available bandwidth
- ❑ Unfortnulately, the mid-band FR3 is densely populated by other services (mostly radars) thus the available spectrum is largely **disaggregated**

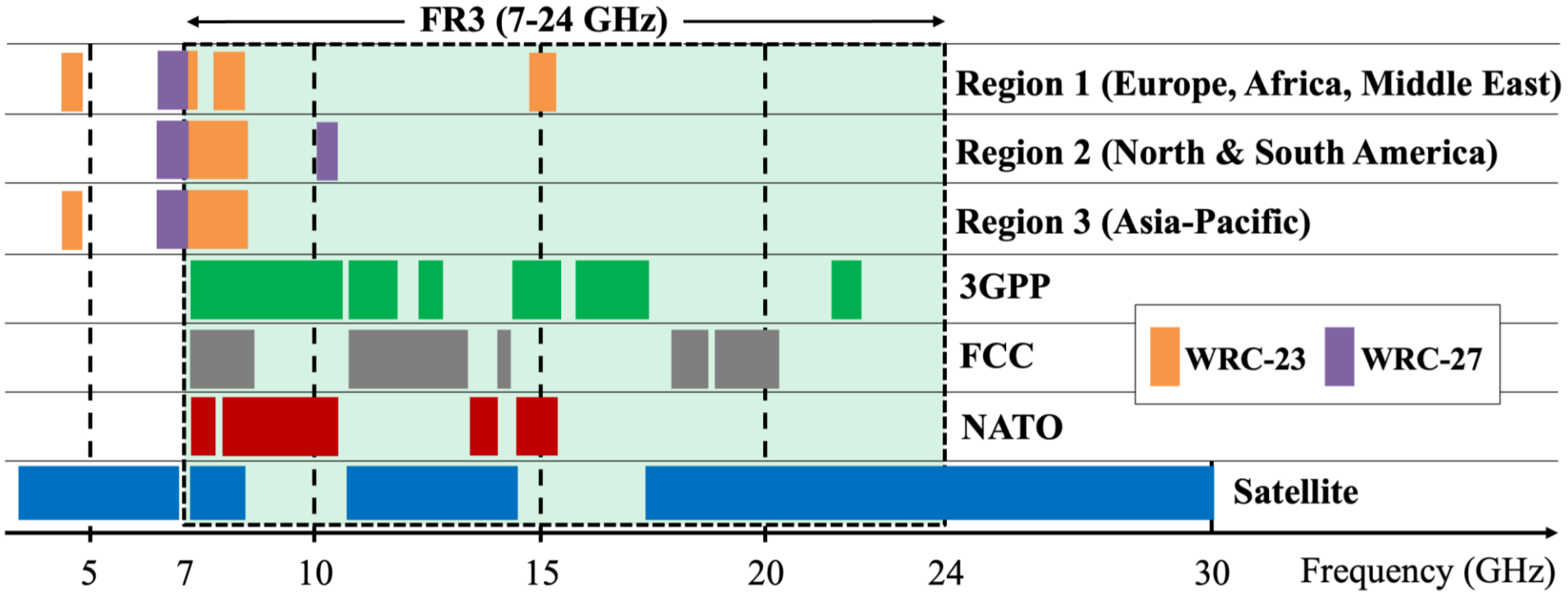

Jacopo Pegoraro and Gianmaria Ventura and Dario Tagliaferri and Marco Mezzavilla and Andrea Bedin and Michele Rossi and Joerg Widmer, **Toward Multiband Sensing in FR3: Frequency Anisotropy Characterization and Non-Contiguous Bands Aggregation Algorithms**, accepted for publication

Potential for high-resolution sensing

Multi-band sensing @FR3 shows great potential to increase range resolution but suffers from:

1. **Phase incoherence** across subbands
   - ❑ Due to hardware (can be compensated)
   - ❑ **Due to target (CANNOT be compensated)**
2. **Grating lobes** of the range ambiguity function due to frequency gaps

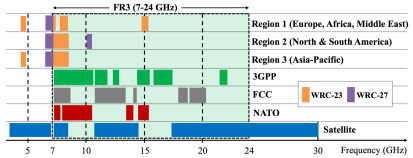

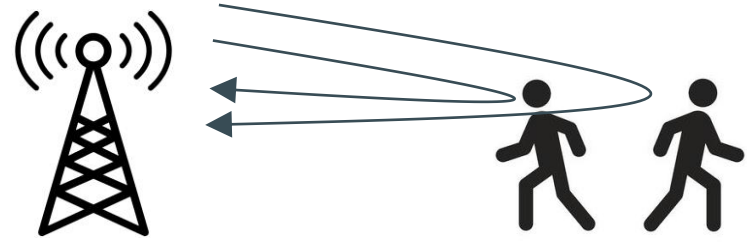

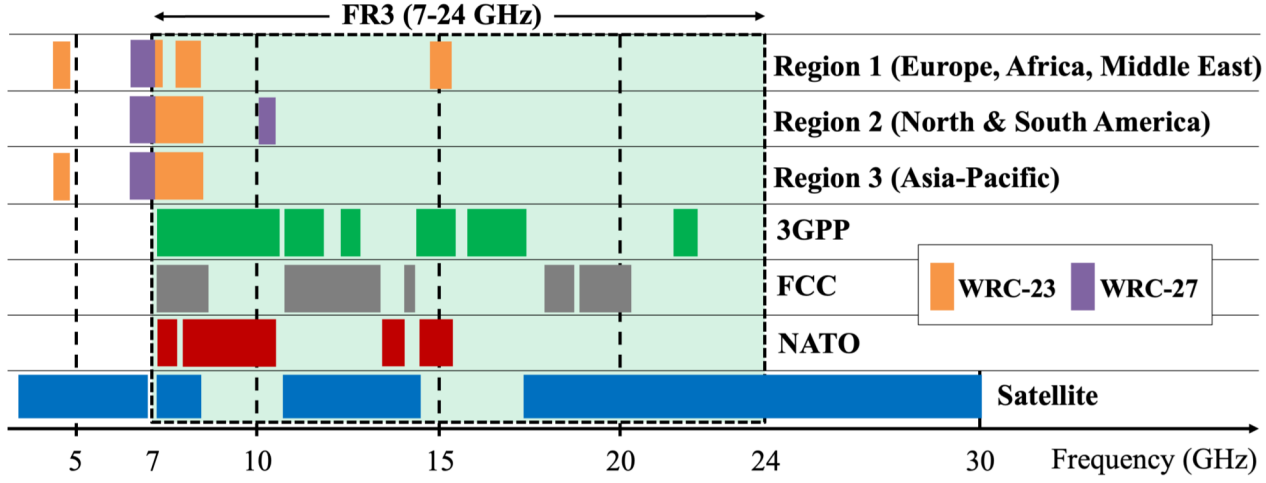

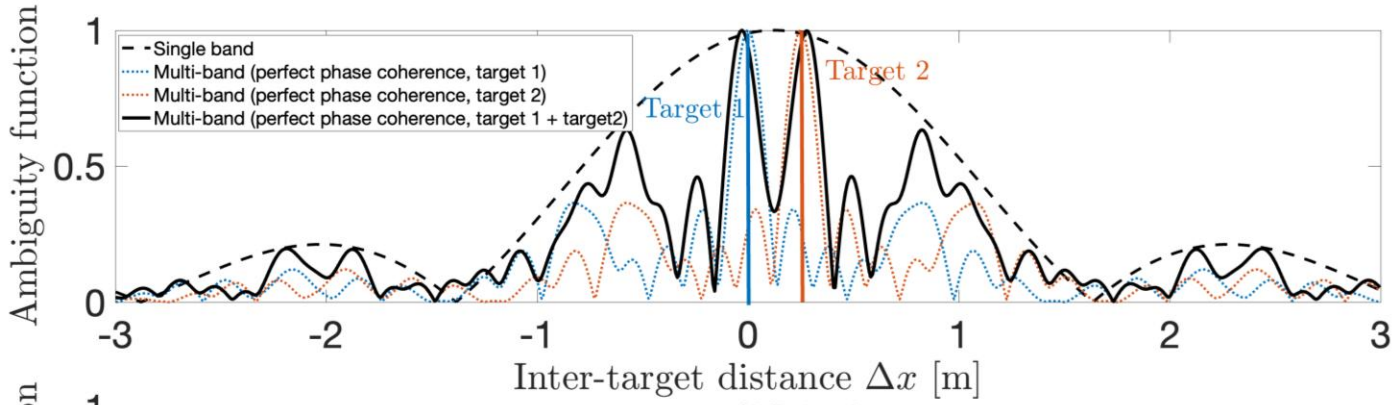

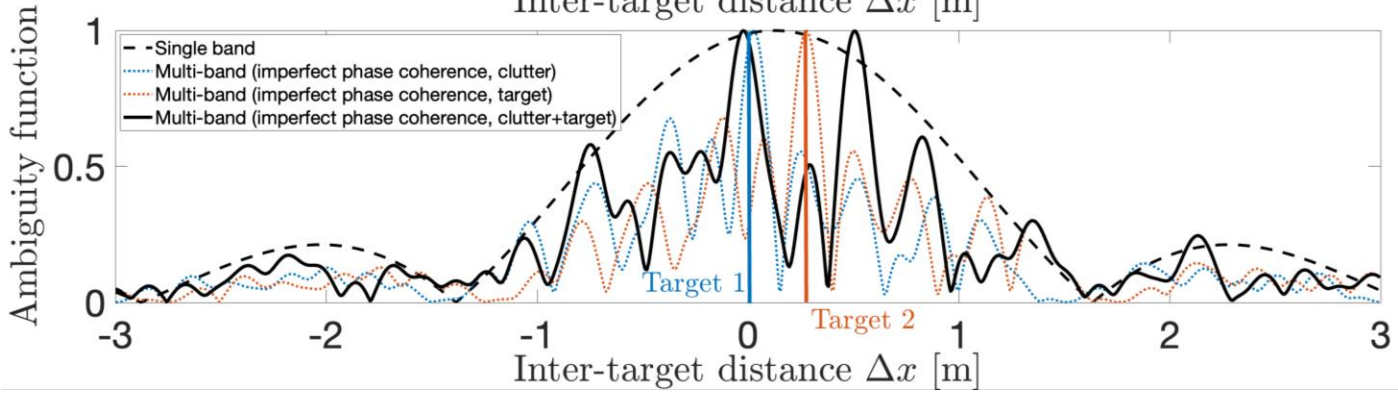

N. Gonzalez-Prelcic, D. Tagliaferri, M. F. Keskin, H. Wymeersch, and L. Song, **Six integration avenues for ISAC in 6g and beyond**, IEEE Vehicular Technology Magazine, vol. 20, no. 1, pp. 18–39, 2025

Outline

1. **Radio imaging in ISAC systems**
   - Brief recall of fundamentals
   - Methods (linear and non-linear)
   - Coherent multistatic imaging and integration into ISAC

2. **Multi-band sensing at FR3**
   - Motivation, potential and challenges
   - Frequency anisotropy characterization

Frequency anisotropy of targets

Real targets are often multi-layer structures with frequency-dependent EM properties

The **effective penetration depth** within the object depends on frequency (skin effect + multi-layer)

Let us consider a monostatic OFDM ISAC signal with K subbands, each with N subcarriers, L targets

$$x_k(t) = \sum_{n=-\frac{N_k}{2}}^{\frac{N_k}{2}-1} a_n e^{j2\pi n\Delta_f t} e^{j2\pi f_k t}$$

Expected (ideal) Rx signal

$$y_k(t) = \sum_{\ell=1}^{L} \rho_\ell e^{j\theta_\ell} \sum_{n=-\frac{N_k}{2}}^{\frac{N_k}{2}-1} a_n e^{-j2\pi(f_k+n\Delta_f)\tau_\ell} e^{j2\pi n\Delta_f t} + z_k(t)$$

Real Rx signal

$$y_k(t) = \sum_{\ell=1}^{L} \rho_{\ell,k} e^{j\theta_{\ell,k}} \sum_{n=-\frac{N_k}{2}}^{\frac{N_k}{2}-1} a_n e^{-j2\pi(f_k+n\Delta_f)\tau_{\ell,k}} e^{j2\pi n\Delta_f t} + z_k(t)$$

The delay depends on k, as well as the scattering phase

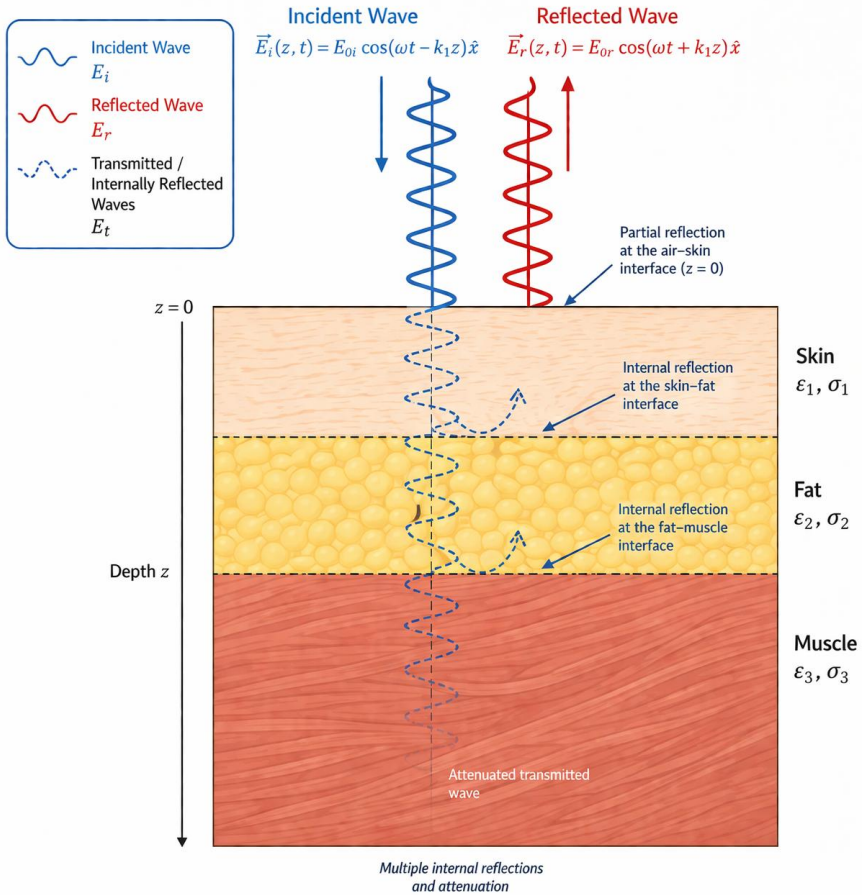

Frequency anisotropy of targets

Approximate Rx signal (frequency anisotropy as a phase effect)

$$y_k(t) \approx \sum_{\ell=1}^{L} \rho_{\ell,k} e^{j\theta_{\ell,k}} \sum_{n=-\frac{N_k}{2}}^{\frac{N_k}{2}-1} a_n e^{-j2\pi(f_k+n\Delta_f)\tau_\ell} e^{j2\pi n\Delta_f t} + z_k(t)$$

Estimated CIR

$$\widehat{h}_k(t) = \sum_{\ell=0}^{L} \rho_{\ell,k} e^{j\theta_{\ell,k}} \mathrm{sinc}\left[B_k(t-\tau_\ell)\right] e^{-j2\pi f_k \tau_\ell} + w_k(t)$$

Phase-compensated CIR

$$\eta_k(R) = \widehat{h}_k\left(\frac{2R}{c}\right) e^{j\frac{4\pi f_k}{c}R}$$

$$= \sum_{\ell=0}^{L} \rho_{\ell,k} e^{j\theta_{\ell,k}} \underbrace{\mathrm{sinc}\left[\frac{2B_k}{c}(R-R_\ell)\right]}_{\chi_k(R-R_\ell)} e^{j\frac{4\pi f_k}{c}(R-R_\ell)} + w_k(R)$$

Range ambguity function

The **effective penetration depth** ranges from few mm to 1-2 cm in FR3

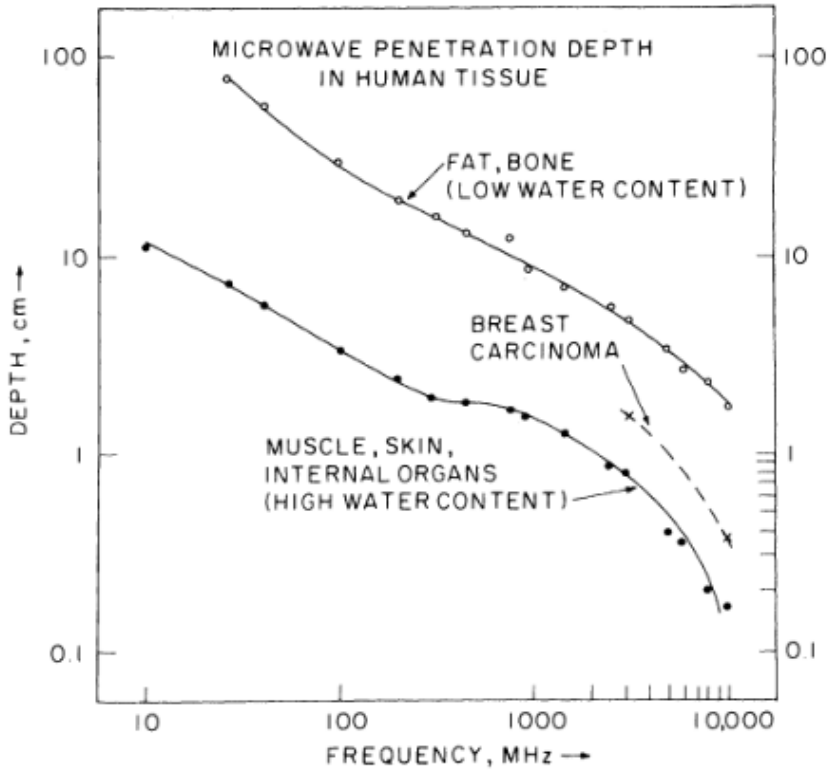

Image courtesy from: Barrett, Alan H., and Philip C. Myers. **Subcutaneous Temperatures: A Method of Noninvasive Sensing.** *Science*, vol. 190, no. 4215, 1975, pp. 669–71. *JSTOR*, http://www.jstor.org/stable/1741200. Accessed 15 Apr. 2026.

Characterization of frequency anisotropy over FR3 spectrum

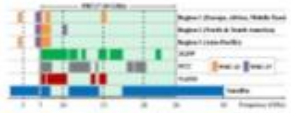

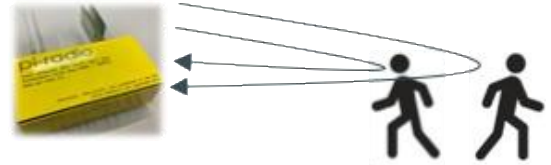

Pi-Radio FR3 board: 2x2 MIMO from 6.5 to 22.5 GHz

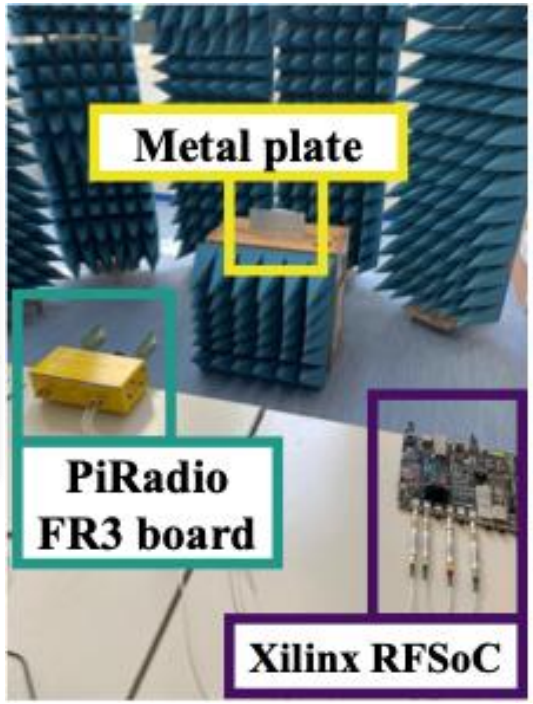

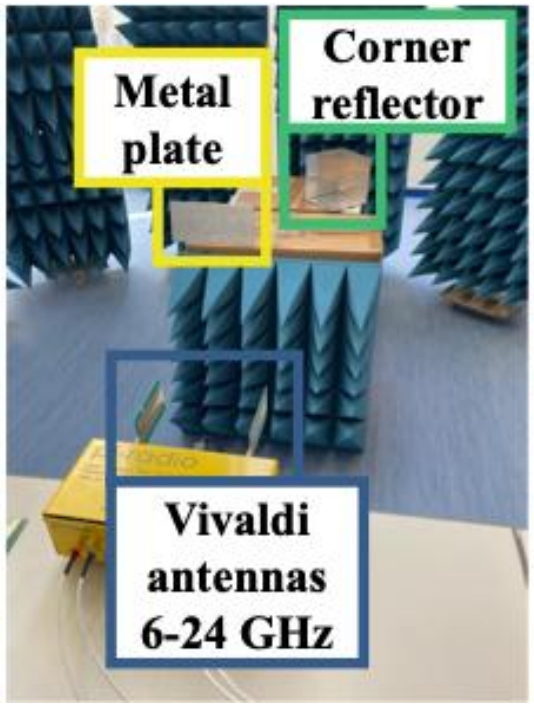

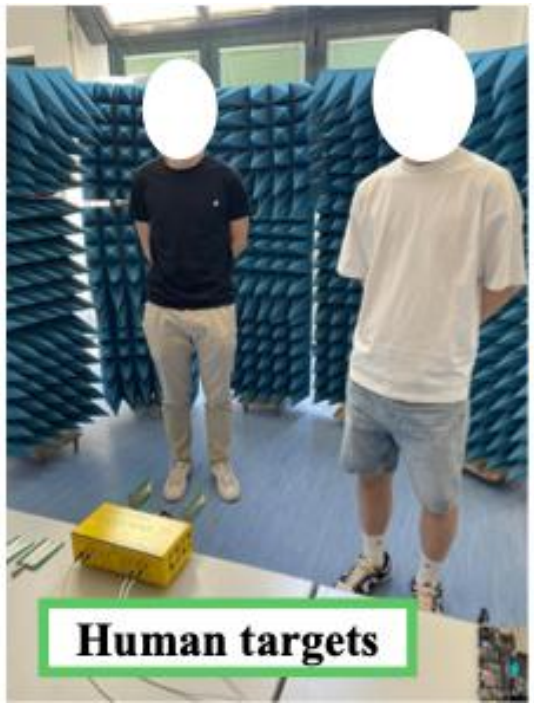

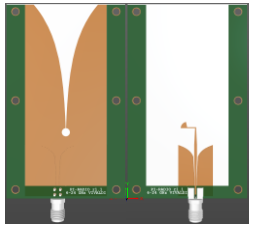

Vivaldi antennas emitting from 6.5 to 22.5 GHz

Characterization of frequency anisotropy over FR3 spectrum

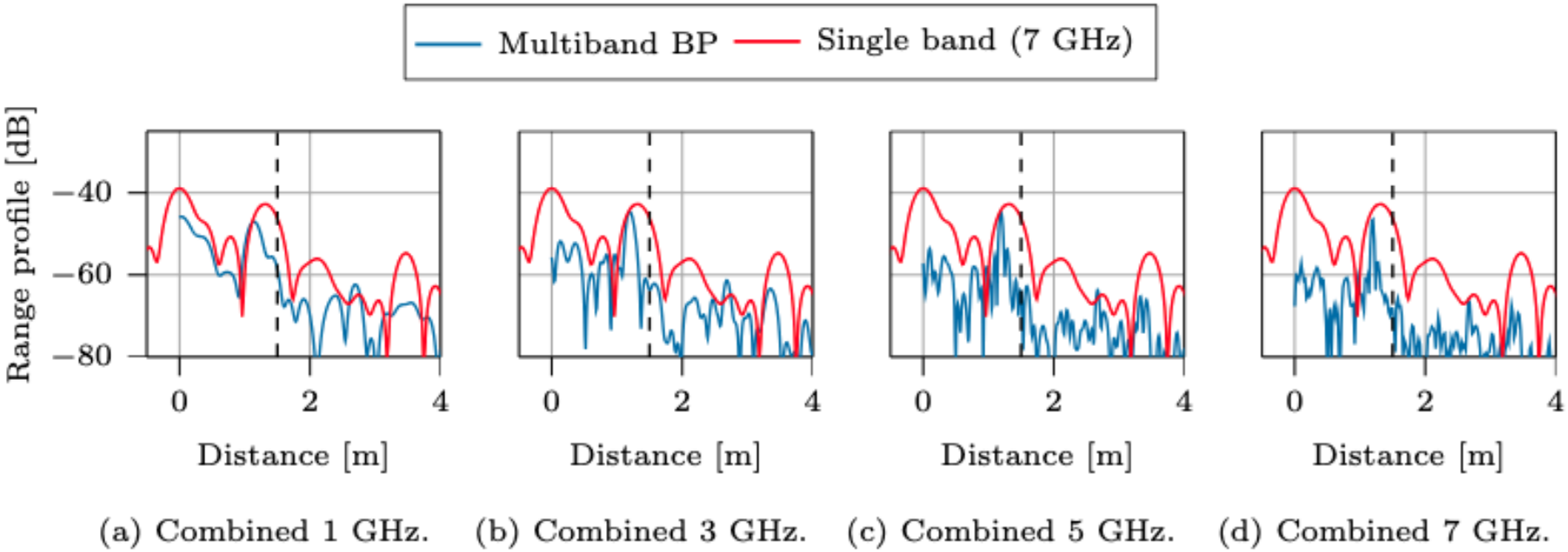

(a) Combined 1 GHz. (b) Combined 3 GHz. (c) Combined 5 GHz. (d) Combined 7 GHz.

Example from experiments: multiband coherent CIR for a metal corner reflector reflector

Multiband phase coherence

$$\mathrm{MPC}(\ell) = \left| \frac{1}{K} \sum_{k=0}^{K-1} e^{j \angle \eta_k(R_\ell)} \right|$$

Normalized Multiband peak magnitude

$$\mathrm{NMPM}(\ell) = 20 \log_{10} \left(\frac{|\eta(R_\ell)|}{\frac{1}{K} \sum_{k=0}^{K-1} |\eta_k(R_\ell)|} \right)$$

Effective multiband peak width

$$\mathrm{EMPW}(\ell) = \{R \,|\, \eta(R) \geq \eta(R_\ell)/2\}$$

Jacopo Pegoraro and Gianmaria Ventura and Dario Tagliaferri and Marco Mezzavilla and Andrea Bedin and Michele Rossi and Joerg Widmer, **Toward Multiband Sensing in FR3: Frequency Anisotropy Characterization and Non-Contiguous Bands Aggregation Algorithms**, accepted for publication

Characterization of frequency anisotropy over FR3 spectrum: example

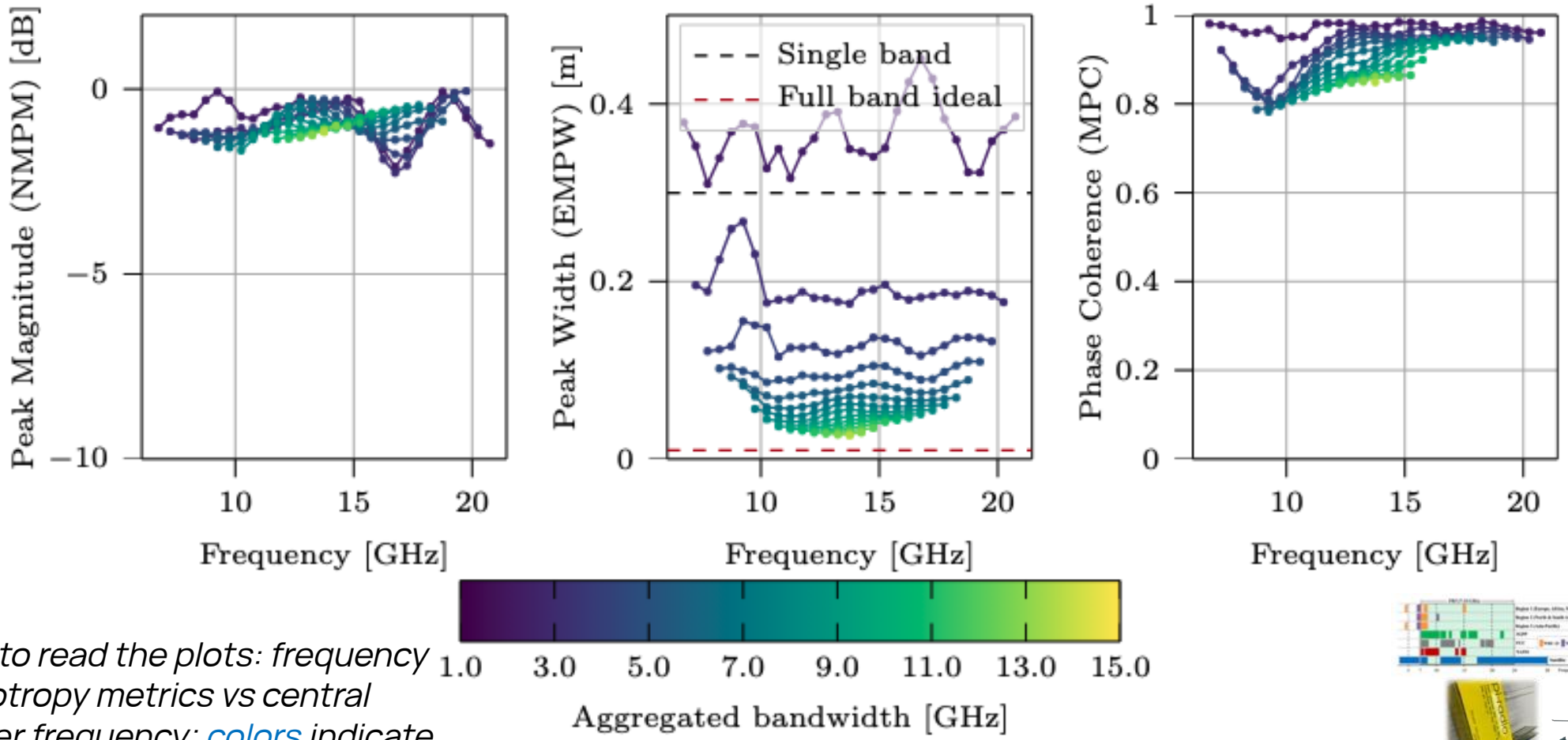

Frequency anisotropy metrics for a corner reflector: it is practically phase coherent over very wide frequency ranges (up to 10-12 GHz) as expected

How to read the plots: frequency anisotropy metrics vs central carrier frequency; colors indicate the total multiband coherently aggregated

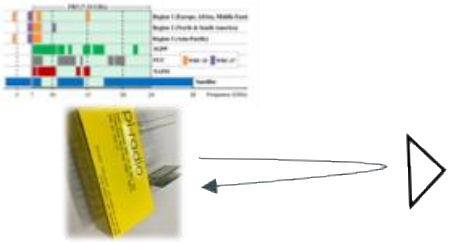

Jacopo Pegoraro et al, **Toward Multiband Sensing in FR3: Frequency Anisotropy Characterization and Non-Contiguous Bands Aggregation Algorithms**, accepted for publication

Characterization of frequency anisotropy over FR3 spectrum: example

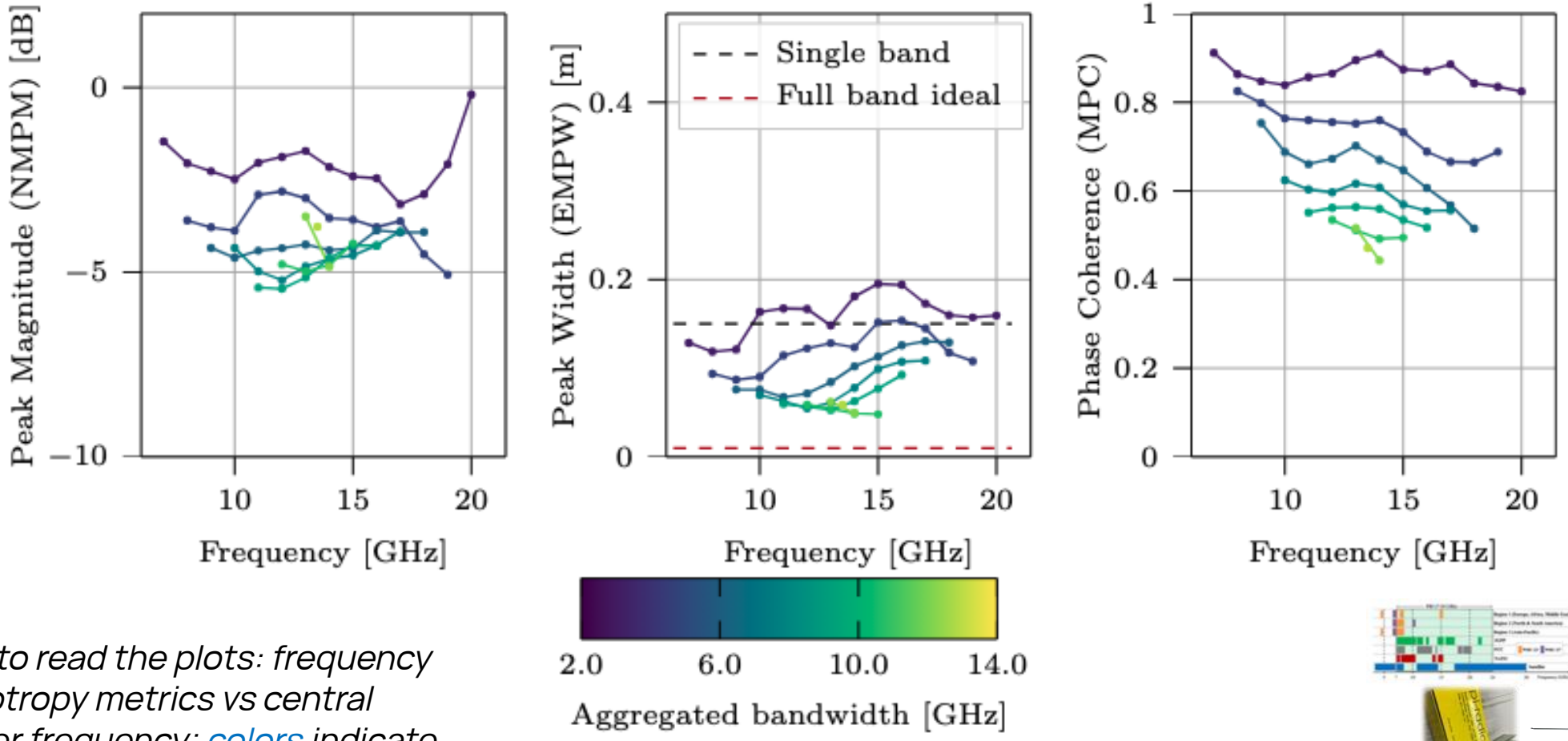

Frequency anisotropy metrics for a **human target**: it is practically phase coherent over 3-4 GHz at 8 GHz, while it is coherent over 2 GHz at 15 GHz

How to read the plots: frequency anisotropy metrics vs central carrier frequency; colors indicate the total multiband coherently aggregated

Jacopo Pegoraro et al, **Toward Multiband Sensing in FR3: Frequency Anisotropy Characterization and Non-Contiguous Bands Aggregation Algorithms**, accepted for publication

Outline

1. **Radio imaging in ISAC systems**
   - Brief recall of fundamentals
   - Methods (linear and non-linear)
   - Coherent multistatic imaging and integration into ISAC

2. **Multi-band sensing at FR3**
   - Motivation, potential and challenges
   - Frequency anisotropy characterization
   - Multi-band ranging

Multi-band ranging

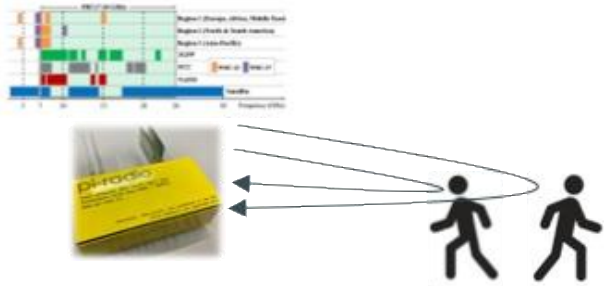

The theoretical resolution is high, but the ***effective*** one is hindered by grating lobes

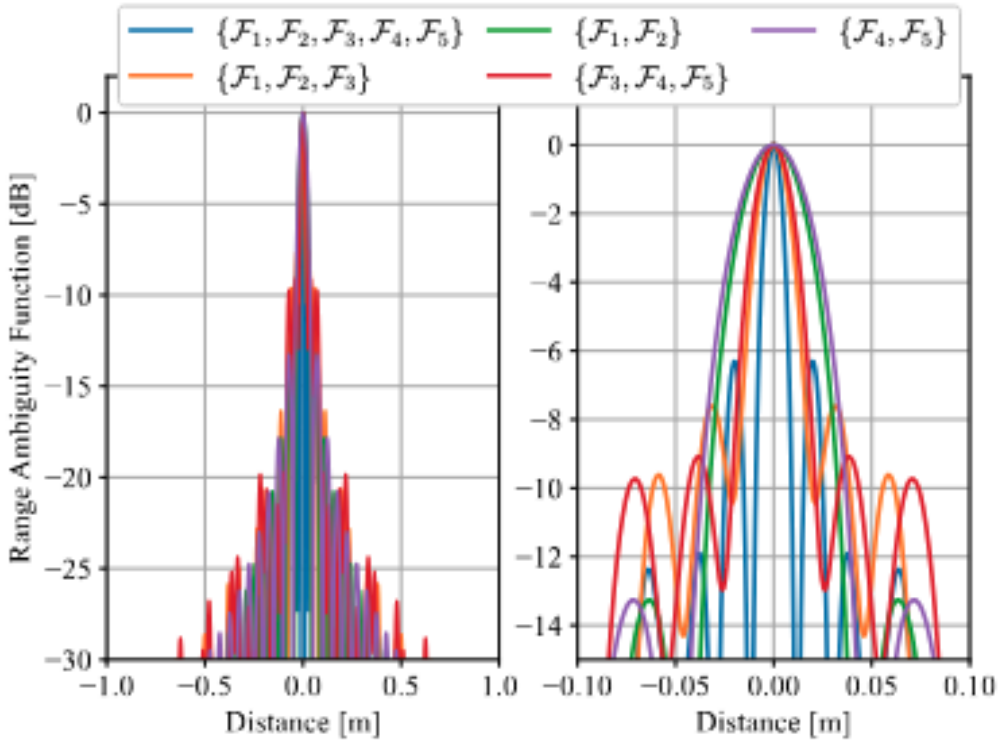

(a) Multiband RAF (left), and zoom on the main peak (right).

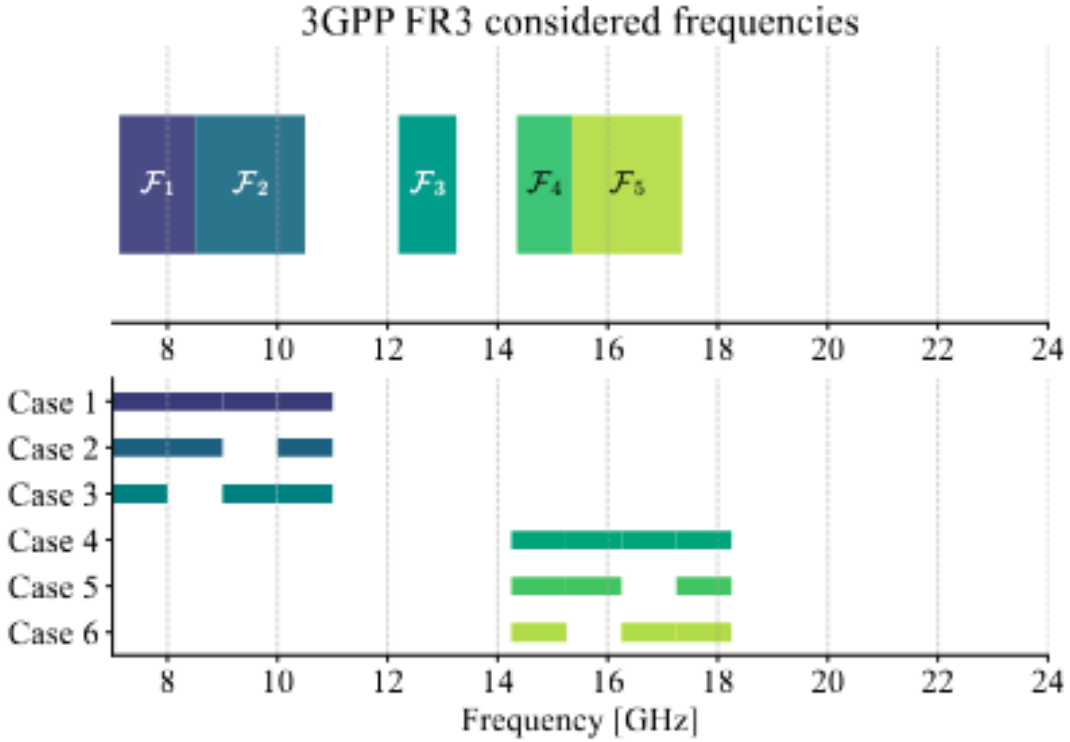

(b) 3GPP FR3 considered frequencies (top) and our considered subbands in case of human targets (bottom).

Multi-band ranging methods

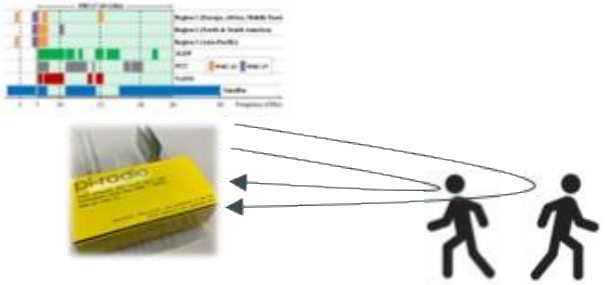

- Backprojection (BP)

$$\eta_{\mathrm{BP}}(R) = \sum_{k=0}^{K-1} \eta_k(R)$$

Coherent summation of phase-compensated CIRs over **all the bandwidths for which the target is frequency-isotropic**

- Subset product BP (SPBP)

$$\eta_{\mathrm{SPBP}}(R) = \left(\sum_{k \in \mathcal{K}_0} \eta_k(R) \right) \cdot \left(\sum_{k \in \mathcal{K}_1} \eta_k(R) \right)$$

Multiplication of two coherent CIRs, over two subsets of bandwidths in order **to maximize PSLR**

- Non-coherent

$$\eta_{\mathrm{NC}}(R) = \sum_{k=0}^{K-1} |\eta_k(R)|$$

- Orthogonal Matching Pursuit (OMP)

Jacopo Pegoraro and Gianmaria Ventura and Dario Tagliaferri and Marco Mezzavilla and Andrea Bedin and Michele Rossi and Joerg Widmer, **Toward Multiband Sensing in FR3: Frequency Anisotropy Characterization and Non-Contiguous Bands Aggregation Algorithms**, accepted for publication

Multi-band ranging results

Exemplary range profiles for two **human targets** (7-11 GHz)

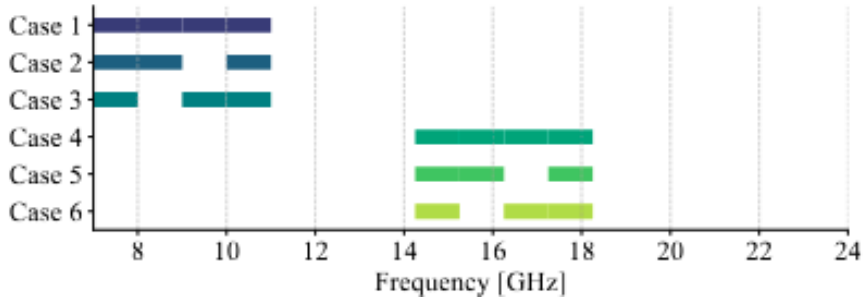

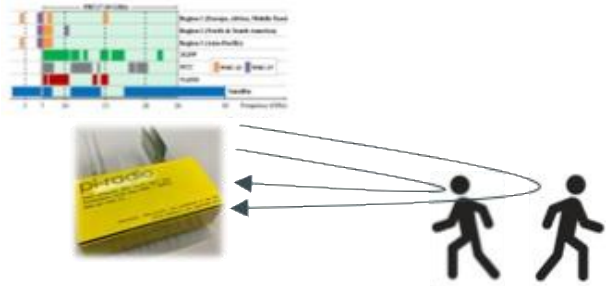

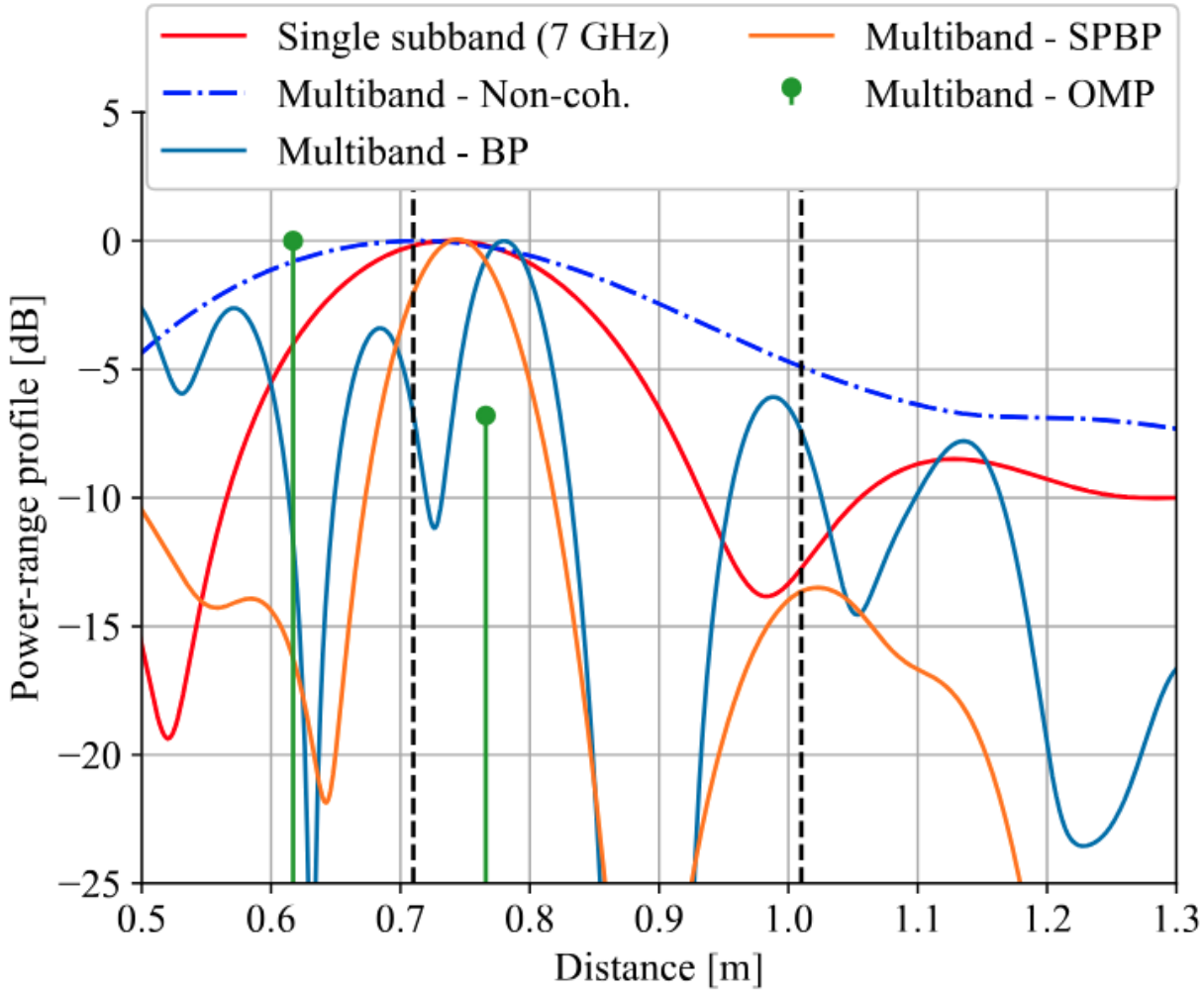

Grating lobes are highly mitigated by the used of non-linear processing (SPBP)

There is a trade-off between PSLR and SNR for the weaker targets that need to be accounted for

Multi-band ranging results

Two **human targets**

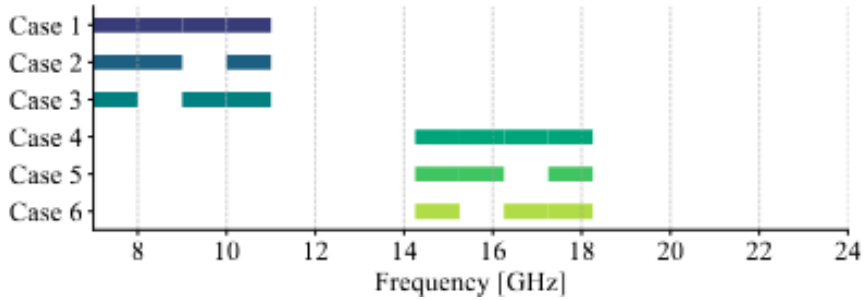

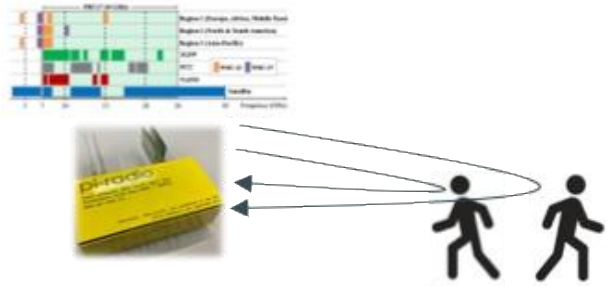

On average, SPBP is more accurate in estimating the true number of targets

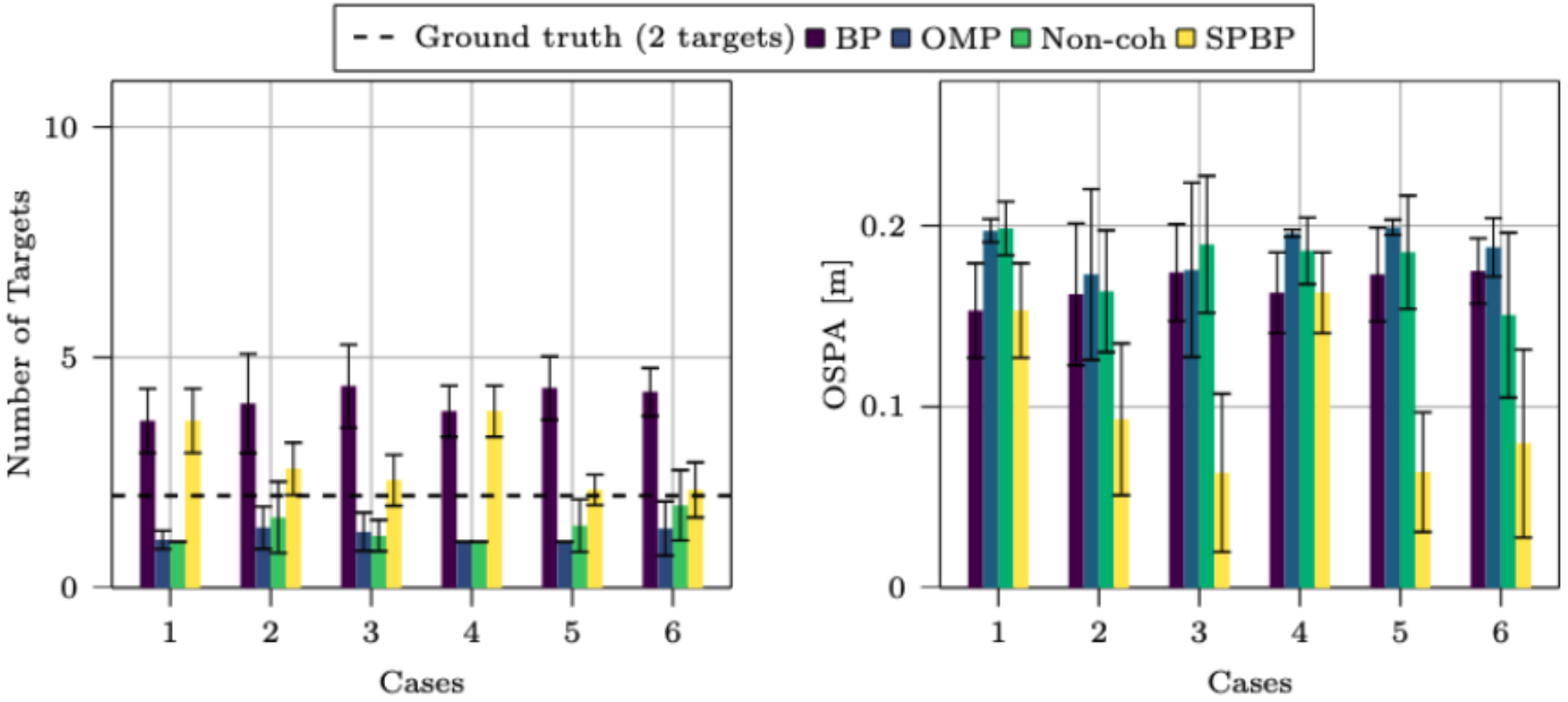

(a) Number of targets detected.

(b) OSPA.

The average OSPA is slightly higher in cases 4,5,6, confirming that human targets are less coherent at higher frequencies

Final thoughts

1. Imaging has the potential of becoming a killer sensing technology in 6G and beyond wireless systems, but it requires **much more experimentation and research to find killer applications**
2. The integration of imaging into communication system would enable pervasive coverage and high resolution through coherent cooperation, but **calibration is challenging**

3. FR3 multi-band systems are an interesting topic of research for next few years, **provided that new bands beyond 6-7 GHz are actually unlocked**
4. Ranging resolution is limited by target nature. **Frequency anisotropy poses a hard limit on coherent aggregation that cannot be overcome**

Thanks